Exploiting Beam-Split Effect in IRS-Aided Systems via Opportunistic OFDMA: Design and Analysis

L. Yashvanth, and Chandra R. Murthy, *Fellow, IEEE*

***Abstract*—This paper addresses the challenges caused by employing phased-array-based intelligent reflecting surfaces (IRSs) for wideband beamforming applications at mmWave frequencies. When a large IRS is used in conjunction with a wideband signal, a phenomenon known as the beam-split (B-SP) effect arises wherein the IRS fails to focus its reflected energy toward a single user equipment (UE) across the entire signal bandwidth, resulting in a dramatic reduction in array gain and throughput. While B-SP is commonly regarded as a performance-limiting impairment, in this paper, we take an optimistic viewpoint and exploit the B-SP to improve system performance using orthogonal frequency division multiple access (OFDMA). We first show that, under the B-SP effect, the IRS can inherently exhibit a *multi-directional beamforming* behavior, directing its energy toward different spatial angles at different frequency components. Capitalizing on this property, we then propose an opportunistic OFDMA scheme wherein the IRS phase shifts are randomly configured, and multiple UEs are *opportunistically* scheduled over different subcarriers (SCs) using a max-rate scheduling policy. We rigorously prove that, when the number of UEs is large, the B-SP can almost surely procure the optimal array gain on all SCs (possibly at different UEs). Subsequently, we characterize a sufficient condition on the number of UEs to witness near-optimal gains in practical systems. Then, we demonstrate that the proposed OFDMA scheme offers multi-user diversity benefits, resulting in further throughput enhancements beyond those achieved through optimal beamforming. Finally, we also show how our idea extends to near-field propagation scenarios. Numerical simulations reveal that the OFDMA scheme outperforms the existing IRS-aided wideband beamforming solutions at low cost and complexity.**

***Index Terms*—Intelligent reflecting surface, opportunistic communication, OFDMA, beam split, multi-user diversity.**

I. Introduction

Intelligent reflecting surfaces (IRSs) are envisioned to enhance the throughput of next-generation wireless systems [2], [3]. An IRS comprises numerous passive elements that apply controllable phase shifts to manipulate the wireless channel between nodes. By appropriately configuring these phase angles, the IRS can coherently combine the signal copies at the receiver (e.g., a user equipment (UE)), thereby improving the signal-to-noise ratio (SNR) and throughput. In high-frequency bands such as millimeter waves (mmWaves), where the propagation losses are severe, IRSs can help to enhance the channel quality [4], [5]. However, a large number of IRS elements is typically required to overcome the multiplicative path loss experienced in the cascaded base station (BS)-IRS-UE channel. In such cases, the propagation delay of the signal across the IRS aperture may become comparable or even exceed the sampling duration, leading to the *spatial-wideband* (SW) effect, and, consequently, the *beam-split* (B-SP) effect in the frequency domain [6]. This paper rigorously analyzes how the B-SP effect alters the directional response of an IRS and proposes an opportunistic orthogonal frequency division multiple access (OFDMA) scheme that exploits the B-SP to enhance system performance.

A. Challenges, Importance and Novelty

A key objective of the next-generation wireless systems is to deliver enhanced mobile broadband (eMBB) connectivity to all devices, and one way to facilitate this is to perform communications in high-frequency bands like mmWave, where abundant spectrum is available, which can enhance the data rates [7]. However, mmWave signals suffer from severe propagation losses, which degrade the SNR and limit the coverage. To address this, IRSs have been proposed to create *virtual line-of-sight* (LoS) links between the BS and UE, thereby improving the signal strength [8]. As explained before, an IRS consists of numerous passive elements with individually tunable phase shifts that allow for constructive combining of the signals at the UE, in turn providing a beamforming/array gain. A large number of IRS elements is typically used to provide sufficient beamforming gain to compensate for the high path losses [9]. However, when a wide bandwidth (BW) is used in conjunction with a large IRS array, the signal propagation delay across the IRS aperture can become comparable to or exceed the sampling period, even under LoS settings. This violates the narrowband condition and leads to a multi-tap channel in the time domain, and causes the *beam-split* (B-SP) effect, where the IRS fails to focus its beam at a given UE over the entire BW, thereby degrading the array gain and throughput [6], [10], [11].

Addressing the B-SP effect at the IRS is generally challenging because phase shifters can only approximate delays under narrowband conditions, where beamforming by controlling the phases is effective [12]. In wideband regimes, this approximation breaks down, making it difficult for an IRS to coherently beamform across the entire bandwidth. This reduction in array gain is a fundamental consequence of the fact that IRSs use phase shifters for beamforming. Thus, it is important and non-trivial to mitigate the B-SP effect for two main reasons: (a) the B-SP effect undermines the core advantage of using an IRS for enhancing the throughput in mmWave bands, and (b) existing solutions for mitigating B-SP in conventional antenna arrays cannot be directly applied to an IRS due to the passive nature and associated hardware & power constraints at the IRS.

L. Yashvanth is with Dept. of EEE, University College London, WC1E 6BT London, U.K. He was with Dept. of Electrical Communication Engineering (ECE), Indian Institute of Science, Bengaluru, India 560 012, during the development of this work. E-mail: yashvanthl@iisc.ac.in.

C. R. Murthy is with the Dept. of ECE, Indian Institute of Science, Bengaluru, India 560 012. E-mail: cmurthy@iisc.ac.in.

This work was financially supported in parts by the Prime Minister's Research Fellowship (PMRF), Govt. of India, and Qualcomm 6G UR India Grant. This paper was presented in part at the 50th IEEE International Conf. on Acoustics, Speech, and Signal Processing (ICASSP), Apr. 2025 [1].

As explained in the sequel, most prior work treats the B-SP effect as detrimental and advocates solutions to suppress it. In our work, we adopt a novel perspective wherein we propose a new scheme that exploits the B-SP effect, while still limiting the loss of array gain and improving the system performance.

B. Related Work

First, most of the existing work on IRS-aided mmWave systems ignores B-SP-induced impairments (e.g., [4], [5], [8]), and hence overestimates the performance of IRS-aided wideband systems. This literature survey focuses on papers discussing wideband effects in IRS-aided systems.

Considering beam-squint (B-SQ), a milder form of the B-SP effect, channel estimation and beam training methods were proposed in [13], [14], while [15] explored UE localization. IRS phase optimization to maximize sum-rate in orthogonal frequency division multiplexing (OFDM) systems was considered in [16], and joint design of IRS and BS precoding for multiple-input multiple-output (MIMO) terahertz systems was studied in [17], [18]. The ergodic rate performance of MIMO-OFDM under B-SQ was analyzed in [19], signal-to-interference-plus-noise ratio (SINR) maximizing design of IRS configurations were derived in [20], and in [21], phase shifts are optimized to adjust the beam widths of the IRS in an OFDMA framework. Along the lines of mitigating the SW effect, existing works often use true time-delay (TTD) units at the IRS to compensate for the excess signal delay across the aperture, thereby eliminating the SW effects [10]. In [11], the design of TTD-enabled IRS was investigated, [22] considered the use of delay-phase units to eliminate the B-SP effects in both far-field and near-field scenarios, and in [23], the TTDs and BS precoder were jointly optimized to maximize the sum-rate of a multi-user system. However, equipping an IRS with TTD units is impractical for the following reasons: 1) the number of required TTD components scales linearly in the number of IRS elements, leading to higher hardware complexity and a larger physical area, 2) it incurs more power consumption due to the necessity for precise delay compensation using high-resolution delay lines, and 3) the full-duplex operation inherent to TTD-enabled IRS elements, where each element must simultaneously receive the BS signal, apply a delay, and retransmit it toward the UE, necessitates a self-interference cancellation mechanism [24]. To the best of our knowledge, no prior work has demonstrated a practical hardware implementation of a TTD-enabled IRS. Therefore, while TTD compensation removes differential delays across the IRS aperture and facilitates a genie-aided evaluation of the achievable rate, it does not constitute a practically feasible solution. Similarly, hybrid analog-digital beamforming techniques, which are used to mitigate the B-SP effect at the BS antenna arrays [25], are not applicable to IRSs, since IRS elements are strictly passive and lack radio-frequency (RF) chains and baseband processing capabilities. Finally, in our prior work [26], we show that instead of a TTD-based IRS, appropriately splitting a large IRS into multiple distributed IRSs and placing them at carefully chosen locations can naturally mitigate the B-SP effects without compromising on the performance and has low complexity. However, this approach targets scheduling a single UE across the entire BW, and the effectiveness of it to mitigate the B-SP critically depends on the placement of IRSs relative to the BS and UE locations. Hence, this solution is well suited for scenarios where a single UE or a cluster of UEs, such as those in a small, dense hotspot; however, it is less effective when the UEs may be arbitrarily located.

In contrast with the above approaches, which aim to mitigate the B-SP effect, this paper explores an opportunistic OFDMA scheme that takes an optimistic view of the B-SP effect and leverages it to enhance system performance through randomly configured IRS phase shifts. Although [27], [28] address problems related to IRS-assisted OFDMA, they focus on sub-6 GHz bands where B-SP effects are not significant.

C. Theoretical Contributions of This Paper

By revisiting the modeling of a large IRS-aided mmWave wideband system from first principles, we first formalize the emergence of the B-SP effect and its impact on the achievable array gain across the operating BW. Building on this, we establish the following six main theoretical contributions:

1) **Directional response**: When the IRS is tuned to reflect in a specific direction at one frequency, it necessarily reflects toward other angles at neighboring frequencies of the BW. A closed-form characterization of this frequency-dependent directional response is provided in Lemma 1.
2) **Multi-directional beamforming**: Next, in Lemma 2, we identify the sub-BW over which the IRS focuses in a given direction within the half-power beamwidth. Using this, in Theorem 1, we derive the number of resolvable beams formed by the IRS simultaneously over disjoint sub-bands of the system BW under the B-SP effect.
3) **Exploiting B-SP effect**: In Theorem 2, we demonstrate that, with a large number of UEs and randomized IRS phase coefficients drawn from a suitable distribution, at least one UE will almost surely achieve the full IRS array gain on every subcarrier (SC) under the B-SP effect.
4) **Scaling of number of UEs**: In Proposition 1, we derive a sufficient scaling on the number of UEs required to achieve near-optimal array gain across the entire BW. In particular, we show that the required number of UEs scales linearly with the number of resolvable IRS beams.
5) **Rate-scaling law with opportunistic OFDMA**: In Theorem 3, we derive the achievable system throughput under a max-rate scheduler and show that our method not only exploits the B-SP effect and delivers full array gain on every SC but also harnesses multi-user diversity benefits over the BW to further enhance performance.
6) **Extensions to near-field scenarios**: Finally, we show that under the B-SP effect in near-field scenarios, an opportunistic OFDMA obtains the full beamfocusing gain across the BW by scheduling a UE whose angle-distance pair is best matched with the randomized IRS phase.

D. Key Insights and Qualitative Takeaways

Our theoretical developments offer many important insights:

- The B-SP effect, traditionally viewed as detrimental, inherently redistributes energy across different spatial directions due to *the law of conservation of energy*. This implies that when the IRS fails to beamform toward a single UE at a given frequency, it must redirect energy toward other UEs in different directions at other frequencies, thereby enabling multi-directional beamforming (BF).
- Our results demonstrate that with a sufficient number of UEs, even a randomized IRS configuration, along with opportunistic scheduling, can exploit the multi-directional BF property of the B-SP effect and provide full BF gain across the entire BW without IRS optimization overheads.
- Our method is applicable to both far-field and near-field wireless systems.
- In terms of practical relevance, in a system with a 1024-element IRS operating over a 400 MHz bandwidth at 30 GHz, the proposed opportunistic OFDMA with randomized IRS phases outperforms conventional round-robin (RR) scheduling, which assigns the entire BW to a single UE with IRS phases optimized only for that UE.

Overall, our results demonstrate that even with randomly configured IRS phases and minimal operational overhead, opportunistic OFDMA can substantially mitigate the adverse impact of the B-SP effect from a network-level perspective, offering a low-complexity yet highly effective approach to wideband IRS-assisted communication.

II. System Model and Problem Statement

We consider a downlink wideband mmWave system where a BS equipped with N_t antennas serves K UEs. The system uses OFDM modulation with N SCs spanning a total BW of W centered at a carrier frequency f_c, and is assisted by an M-element IRS to enhance the throughput of the system. We consider that the antenna array at the BS and the IRS are implemented as a uniform linear array (ULA) with inter-element spacing d_{BS}, and d_{IRS}, respectively.[1] For simplicity of exposition, we consider a single antenna at the UEs, and the approach directly extends to multiple antenna UEs also. Further, due to the sparse scattering of signals at mmWave frequencies, we model the channel between the nodes with line-of-sight (LoS) components, as described next.

A. Channel Model

In the downlink mode of the communication, the baseband impulse response of the channel from the n'th antenna at BS to the mth IRS element can be written as [29]

$$g_{n',m}(t) = \alpha_{n',m} e^{-j2\pi f_c \tau^{\mathsf{BI}}_{n',m}} \delta(t - \tau^{\mathsf{BI}}_{n',m}), \tag{1}$$

where $\delta(t)$ is the Dirac-delta function, $\alpha_{n',m}$ corresponds to the large scale channel parameter (accounting for the path loss) from the n'th antenna at the BS to mth element of the IRS, and $\tau^{\mathsf{BI}}_{n',m}$ is the delay in the channel from n'th BS antenna to mth IRS element. Similarly, the impulse response of the channel in the baseband domain from the mth IRS element to UE-k is given by

$$u_{m,k}(t) = \beta_{m,k} e^{-j2\pi f_c \tau^{\mathsf{IU}}_{m,k}} \delta(t - \tau^{\mathsf{IU}}_{m,k}), \tag{2}$$

where $\beta_{m,k}$ and $\tau^{\mathsf{IU}}_{m,k}$ denote the large-scale parameter and delay in the channel from mth IRS element to UE-k, respectively. Thus, the impulse response of the overall channel from the n'th BS antenna to UE-k via the IRS can be written as[2]

$$h_{n'}(t) = \sum\nolimits_{m=1}^{M} \theta_m g_{n',m}(t) \circledast u_{m,k}(t) \tag{3}$$

$$= \sum\nolimits_{m=1}^{M} \theta_m \alpha_{n',m} \beta_{m,k} \delta\left(t - \tau^{\mathsf{BI}}_{n',m} - \tau^{\mathsf{IU}}_{m,k}\right) \times e^{-j2\pi f_c \left(\tau^{\mathsf{BI}}_{n',m} + \tau^{\mathsf{IU}}_{m,k}\right)}, \tag{4}$$

where $\circledast$ denotes the linear convolution operator, and θ_m is the reflection coefficient tuned at the mth IRS element modeled as $\theta_m = \zeta_m e^{j\vartheta_m}$, where ζ_m and ϑ_m denote the amplitude and phase of the reflection coefficient at mth IRS element. For simplicity, we consider that $\zeta_m = 1,\ \forall m \in [M] \triangleq \{1, \ldots, M\}$.

Using the properties of the ULA geometry, the channel delays via the IRS relative to a reference IRS element can be expressed as:

$$\tau^{\mathsf{BI}}_{n',m} = \tau^{\mathsf{BI}_0}_{n'} + \frac{d_{\text{IRS}}}{c}(m-1)\sin(\psi), \tag{5}$$

$$\tau^{\mathsf{IU}}_{m,k} = \eta^{\mathsf{I_0U}}_{k} - \frac{d_{\text{IRS}}}{c}(m-1)\sin(\omega_k), \tag{6}$$

where $\tau^{\mathsf{BI}_0}_{n'}, \eta^{\mathsf{I_0U}}_{k}$ are the signal propagation delays from n'th BS antenna to reference IRS element, and reference IRS element to UE-k, respectively; $c = 3 \times 10^8$ m/s denotes the speed of light; ψ and ω_k represent the direction of arrival (DoA) from the BS and departure (DoD) towards UE-k, respectively, at the IRS. Now, using (5) and (6) in (4), the channel to UE-k from the n'th BS antenna can be simplified as given in (7) at the top of the next page.

Similarly, we express the delay from n'th BS antenna as

$$\tau^{\mathsf{BI}_0}_{n'} = \eta^{\mathsf{BI}_0} + (n'-1)\frac{d_{\text{BS}}}{c}\sin(\chi), \tag{8}$$

where η^{BI_0} is the propagation delay from the reference BS antenna to the reference IRS element, and χ is the DoD at the BS towards the IRS. Let $\eta_k \triangleq \eta^{\mathsf{BI}_0} + \eta^{\mathsf{I_0U}}_{k}$ denote the overall propagation delay from the reference antenna at the BS to UE-k via the reference element of the IRS. Further, since the large-scale path loss is nearly the same across the BS/IRS array, we let $\alpha_{n',m} \approx \alpha$, and $\beta_{m,k} \approx \beta_k \ \ \forall n' \in [N_t], m \in [M]$ [29].

Let $p_{n'}(t)$ denote the response of the transmit precoding filter used at the n'th BS antenna. Then, the effective channel at UE-k is given by

$$h(t) = \sum\nolimits_{n'=1}^{N_t} h_{n'}(t) \circledast p_{n'}(t). \tag{9}$$

Now, using (7) in (9) and simplifying, the final form of $h(t)$ can be obtained as given in (10) on the next page, where $\bar{\alpha} \triangleq \alpha e^{-j2\pi f_c \eta^{\mathsf{BI}_0}}$ and $\bar{\beta}_k \triangleq \beta_k e^{-j2\pi f_c \eta^{\mathsf{I_0U}}_{k}}$ denote the complex channel gain in the BS-IRS and IRS-UE links, respectively.

[1] The ideas pursued in this paper can be directly applied to other types of array geometries at the BS/IRS. For example, in Remark 2, we discuss how the results of this paper extend to a planar array-based geometry.

$$h_{n'}(t) = \sum_{m=1}^{M} \theta_m \alpha_{n',m} \beta_{m,k} \delta\left(t - \tau_{n'}^{\mathsf{BI_0}} - \eta_k^{\mathsf{I_0U}} - \frac{d_{\text{IRS}}}{c}(m-1)\left(\sin(\psi) - \sin(\omega_k)\right)\right) e^{-j2\pi f_c(\tau_{n'}^{\mathsf{BI_0}} + \eta_k^{\mathsf{I_0U}})} \times e^{-j2\pi f_c \frac{d_{\text{IRS}}}{c}(m-1)(\sin(\psi)-\sin(\omega_k))}. \quad (7)$$

$$h(t) = \sum_{n'=1}^{N_t} \sum_{m=1}^{M} \theta_m \bar{\alpha}\bar{\beta}_k \delta\left(t - \eta_k - \frac{d_{\text{BS}}}{c}(n'-1)\sin(\chi) - \frac{d_{\text{IRS}}}{c}(m-1)\left(\sin(\psi) - \sin(\omega_k)\right)\right) \circledast p_{n'}(t) \times e^{-j2\pi f_c\left(\frac{d_{\text{BS}}}{c}(n'-1)\sin(\chi) + \frac{d_{\text{IRS}}}{c}(m-1)(\sin(\psi)-\sin(\omega_k))\right)}, \quad (10)$$

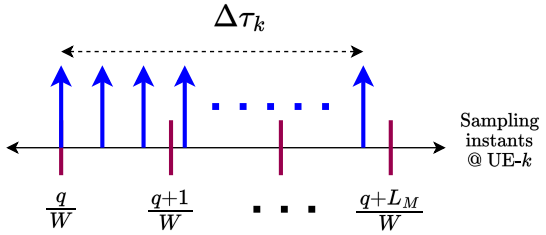

Fig. 1: Illustration of SWE when the SDS $\Delta\tau_k$ spans L_M taps.

B. Spatial-Wideband Effect

The expression for the channel given in (10) corresponds to a multipath scenario where every BS antenna and each IRS element provides a copy of the transmitted signal at the UE. Thus, the *spatial delay spread* (SDS) induced by the channel at UE-k, denoted by $\Delta\tau_k$, is

$$\Delta\tau_k = \frac{d_{\text{BS}}}{c}(N_t - 1)\sin(\chi) + \frac{d_{\text{IRS}}}{c}(M-1)\left(\sin(\psi) - \sin(\omega_k)\right). \quad (11)$$

Clearly, the SDS in the channel at UE-k depends on the DoD at the BS, DoA, and DoD at the IRS: If $\sin(\psi) - \sin(\omega_k) = 0$, and $\chi = 0$, the SDS is 0, and if $\sin(\psi) - \sin(\omega_k) = 2$ and $\chi = 90°$, the SDS takes the maximum value given by $\Delta\tau_{k,\max} = (N_t - 1)\frac{d_{\text{BS}}}{c} + 2(M-1)\frac{d_{\text{IRS}}}{c}$. In general, when the SDS becomes comparable to or exceeds $T_s = 1/W$, the narrowband condition is violated, and the channel becomes frequency-selective, resulting in the spatial-wideband effect (SWE) [6]. The SWE refers to the fact that the delay incurred by the signal while propagating across the aperture of the BS or IRS is comparable to the sampling duration of the signal, and this gives rise to a frequency-selective multi-tap channel (see Figure 1). Note that the SWE arises even with pure LoS paths in the channel. Hence, unlike conventional multipath links, which are characterized by multiple distributed scatterers, the frequency-selective properties under the SWE result in a distinct phenomenon known as the beam-split effect, as described next.

C. The Beam-Split Effect

Owing to the frequency selectivity induced by the SWE, OFDM becomes a natural choice for the transmission of data signals. To this end, applying a Fourier transform to (10), the frequency response of the channel to UE-k on a baseband frequency f (with $|f| \leq W/2$) can be obtained as

[2]We neglect the direct path between the BS and the UEs due to the high attenuation losses faced by the mmWave signals [30], [31, Sec. IV.A].

$$H_k(f) = \bar{\alpha}\bar{\beta}_k e^{-j2\pi f \eta_k} \sum_{n'=1}^{N_t} e^{-j2\pi(f+f_c)(n'-1)\frac{d_{\text{BS}}}{c}\sin(\chi)} P_{n'}(f) \times \sum_{m=1}^{M} e^{-j2\pi(f+f_c)(m-1)\frac{d_{\text{IRS}}}{c}(\sin(\psi)-\sin(\omega_k))} e^{j\vartheta_m}, \quad (12)$$

where the symbols are as defined previously and $P_{n'}(f)$ is the frequency response of the filter $p_{n'}(t)$. Since our goal is to enhance the throughput, maximizing the channel gain in (12) is desirable. In this view, by using the Cauchy-Schwarz inequality, we can obtain $|H_k(f)|^2 \leq |U_k(f)|^2$, where

$$|U_k(f)|^2 \triangleq \left|\bar{\alpha}\bar{\beta}_k N_t\right|^2 \left|\sum_{m=1}^{M} e^{-j2\pi(f+f_c)(m-1)\frac{d_{\text{IRS}}}{c}\sin(\phi_k)} e^{j\vartheta_m}\right|^2, \quad (13)$$

with $\phi_k \triangleq \sin_{(p)}^{-1}\left(\sin(\psi) - \sin(\omega_k)\right)$ being the cascaded channel angle at UE-k via the IRS, and $\sin_{(p)}^{-1}(x)$ is defined such that x lies in the principal argument of the inverse sine function, $[-1, 1)$ [32], [31, Eq. 32]. Note that, for any k, we can achieve the upper bound $|U_k(f)|^2$ in (13) when

$$P_{n'}(f) = e^{j2\pi(f+f_c)(n'-1)\frac{d_{\text{BS}}}{c}\sin(\chi)}, \quad (14)$$

which corresponds to the transmit filter response given by

$$p_{n'}(t) = \delta\left(t + (n'-1)\frac{d_{\text{BS}}}{c}\sin(\chi)\right) e^{j2\pi f_c(n'-1)\frac{d_{\text{BS}}}{c}\sin(\chi)}. \quad (15)$$

Interestingly, the transmit filter achieving the upper bound is independent of the UE being served, so that the full-beamforming gain from the BS array can be obtained using a UE-independent precoding configuration (of course, the array gain achieved does depend on the UE index). We refer the reader to Remark 1 at the end of this section for further details on the implementation of the transmit filter in (15).

Suppose we tune the IRS phase to maximize the channel gain at the centre frequency, $f = 0$, that is, we set

$$\vartheta_m = j2\pi f_c(m-1)\frac{d_{\text{IRS}}}{c}\sin(\phi_k). \quad (16)$$

Then, with $P_{n'}(f)$ chosen as per (14), the overall channel gain on a baseband frequency f with $M > 1$ can be simplified as

$$|H_k(f)|^2 = \left|\bar{\alpha}\bar{\beta}_k N_t\right|^2 \left|\sum_{m=1}^{M} e^{-j2\pi f(m-1)\frac{d_{\text{IRS}}}{c}\sin(\phi_k)}\right|^2$$

$$\overset{(a)}{=} \left|\gamma_k^{\mathsf{C}}\right|^2 M^2 \operatorname{sinc}^2\left(\frac{Mf}{2f_c}\sin(\phi_k)\right), \tag{17}$$

where in (a), we defined $\gamma_k^{\mathsf{C}} \triangleq \bar{\alpha}\bar{\beta}_k N_t$ and the fact that $\sin(x) \approx x$, when $x = \pi f d_{\text{IRS}} \sin(\phi_k)/c \ll 1$; $\operatorname{sinc}(x) \triangleq \frac{\sin(\pi x)}{\pi x}$, and we set $d_{\text{IRS}} = \lambda_c/2$, where λ_c is the carrier wavelength. From (17), we see that unless $f = 0$ or $\phi_k = 0$, the UE experiences a reduced array gain relative to the maximum value of M^2 at other frequency components within the BW; this is known as the *beam-split (B-SP) effect.*

More generally, if we configure the IRS coefficients to form a beam at UE-k on the nth SC of the OFDM system, $n \in [N]$, the overall channel gain at UE-k on frequency f is

$$|H_k(f)|^2 \approx M^2 \left|\gamma_k^{\mathsf{C}}\right|^2 \operatorname{sinc}^2\left(\frac{M(f_n - f)}{f_c}\sin(\phi_k)\right), \tag{18}$$

where $f_n = \frac{nW}{N} - \frac{W}{2} - \frac{W}{2N}$ is the baseband frequency of nth SC. We pictorially illustrate the adverse impact of the B-SP effect in Fig. 2. When the BW, or the number of IRS elements, or both, become large, the resulting degradation in array gain due to the B-SP effect becomes a major limitation in the deployment of IRSs for wideband communication systems.

At this point, we note that the severity of the SWE, and hence the resulting B-SQ/B-SP effects, is not governed solely by the fractional bandwidth (FBW), defined as the ratio of BW to carrier frequency. Instead, it is dictated by the product of the number of IRS elements N and the FBW. For example, as in Fig. 2, with $N = 1024$, $W = 400$ MHz, and $f_c = 30$ GHz, this product is $MW/f_c \approx 13.66$ (i.e., 1366%), which is sufficiently large to induce pronounced B-SP effects at the IRS. Thus, unlike conventional wideband systems, where performance degradation depends primarily on FBW, the onset and severity of the B-SP effect in IRS-assisted systems are determined by the joint scaling of N and the FBW.

D. Problem Statement

From the above discussion, it is evident that the B-SP effect prevents a single UE from achieving the full array gain of M^2 over the entire signal BW. Although the B-SP effect can be mitigated by reducing the number of IRS elements M or the BW W, it has the undesirable consequence of decreasing the overall system throughput. On the other hand, intuitively, if the IRS does not form a beam in a single direction on all SCs, by the *law of conservation of energy*, the reflected energy must necessarily be radiated in different directions across the SCs. In effect, the IRS forms beams pointing towards different UEs in the system across the SCs. Motivated by this, we propose to employ an OFDMA scheme, where different UEs are scheduled across the SCs, thereby *exploiting the B-SP effect*. Specifically, we answer the following:

1) How does the directional response of the IRS vary across the BW under the B-SP effect when IRS configurations are tuned to reflect in a specific direction at a given frequency?[3]
2) Under the B-SP effect, develop and analyze an OFDMA scheme that schedules different UEs on distinct SCs by formulating and solving the following scheduling problem:

Maximize the system throughput obtained over T time slots w.r.t. all schedulers $\mathsf{SCH}(n,t)$, where $\mathsf{SCH} : [N] \times [T] \to [K]$ maps the SC index n and time slot t to UE index k:

$$\max_{\mathsf{SCH}(n,t)} \frac{1}{T}\sum_{t=1}^{T}\sum_{n=1}^{N}\frac{W}{N}\times \log_2\left(1 + \frac{P}{N_t N \sigma^2}|H(\mathsf{SCH}(n,t),t,f_n)|^2\right), \tag{P0}$$

where P is the total transmit power, which is divided equally across the N SCs, σ^2 is the noise variance per SC, and $H(k,t,f)$ is the channel to UE-k at time (slot) t and on frequency f. The factor N_t accounts for the power normalization since the BS is equipped with N_t antennas.

We address these aspects in Secs. III and IV, respectively.

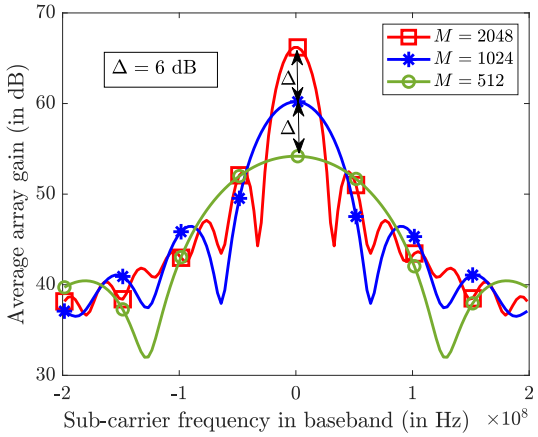

Fig. 2: Average array gain vs. SC frequency when IRS is optimized to $f_n = 0$ for different number of IRS elements, M, with $W = 400$ MHz. Although the gain at $f_n = 0$ increases with M, the gain on other SCs degrades as M increases due to the B-SP effect.

Remark 1 (Using true-time delay units at the BS and IRS)**.** *From (15), we note that each BS antenna applies a timing advance via a TTD unit, which introduces a frequency-dependent phase shift, followed by a frequency-independent phase. While a TTD-enabled array is feasible at the BS, equipping each IRS element with a TTD unit to counteract the SW effect significantly increases hardware complexity and power consumption due to the need for high-precision delays and the requirement of a self-interference cancellation mechanism to handle the full-duplex operation, as explained in Sec. I-B. These practical limitations restrict the applicability of TTDs at the IRS.*

Remark 2 (Extension to other geometry)**.** *The B-SP effect arises regardless of the array geometry employed at the BS or IRS. However, its severity is governed by the number of elements across the array aperture. For e.g., in uniform planar arrays (UPA), elements along the diagonal contribute to the B-SP effects. Accordingly, our proposed ideas and methods generalize to arbitrary array geometries by appropriately scaling the number of elements across the array aperture.*

[3]We note that B-SQ and B-SP effects can arise in both far-field and near-field scenarios [22]. For simplicity of exposition, we first develop the idea and analysis when the BS/UEs are in the far-field of the IRS(s). Subsequently, in Sec. IV-E, we extend our idea to near-field scenarios.

III. Beam-split Enables Multi-Directional Beamforming at the IRS

To accurately characterize the frequency-selective properties of the channel at a UE under the B-SP effect, we first rewrite (13) for $d_{\text{IRS}} = \lambda_c/2$ compactly as follows:

$$|H_k(f)|^2 = \left|\gamma_k^{\mathsf{C}}\right|^2 \left|\boldsymbol{\theta}^H \mathbf{a}_M\left(\sin_{(p)}^{-1}\left\{\left(1+\frac{f}{f_c}\right)\sin(\phi_k)\right\}\right)\right|^2, \tag{19}$$

where $\boldsymbol{\theta} \triangleq \left[e^{-j\vartheta_1}, e^{-j\vartheta_2}, \ldots, e^{-j\vartheta_M}\right]^T$ is the IRS configuration vector (with conjugate phases introduced for notational compactness), and $\mathbf{a}_M(x)$ is the array steering response vector of an M-element ULA oriented at the angle x given by

$$\mathbf{a}_M(x) \triangleq \left[1, e^{-j\pi\sin(x)}, \ldots, e^{-j(M-1)\pi\sin(x)}\right]^T. \tag{20}$$

A. Directional Response of the IRS under B-SP effect

In Lemma 1 below, we determine the directional response of the IRS on the frequencies across the BW of operation when the IRS is tuned to a given frequency within the BW.

Lemma 1. *Let $f_0, \tilde{f}_0 \in [-W/2, W/2]$ be two frequency components within the BW of operation in the baseband domain. If the IRS is configured to reflect in a cascaded spatial direction of ϕ at frequency f_0, then, on frequency $\tilde{f}_0$, the IRS reflects at a cascaded angle $\tilde{\phi}$ given by*

$$\tilde{\phi} = \sin_{(p)}^{-1}\left\{\left(\frac{f_0+f_c}{\tilde{f}_0+f_c}\right)\sin(\phi)\right\}. \tag{21}$$

Proof. From (19), dropping the index k for simplicity, and using the Cauchy-Schwarz inequality, the IRS phase configuration that maximizes $|H(f)|^2$ and reflects the transmitted signal in a cascaded angle of ϕ on frequency f_0 is given by

$$\boldsymbol{\theta}^{\text{opt}} = \mathbf{a}_M\left(\sin_{(p)}^{-1}\left\{\left(1+\frac{f_0}{f_c}\right)\sin(\phi)\right\}\right). \tag{22}$$

To determine the directional response of the IRS vector tuned as per (22) on another frequency $\tilde{f}_0$, we evaluate the beam-scanning function, which is defined as follows.

$$g(\nu) \triangleq \left|\boldsymbol{\theta}^{\text{opt}\,H}\mathbf{a}_M\left(\sin_{(p)}^{-1}\left\{\left(1+\frac{\tilde{f}_0}{f_c}\right)\sin(\nu)\right\}\right)\right|^2 \tag{23}$$

$$= \left|\sum_{m=1}^{M} e^{j\pi(m-1)\left\{\left(1+\frac{f_0}{f_c}\right)\sin(\phi)-\left(1+\frac{\tilde{f}_0}{f_c}\right)\sin(\nu)\right\}}\right|^2 \tag{24}$$

$$= \frac{\sin^2\left(\frac{\pi M}{2}\left\{\left(1+\frac{f_0}{f_c}\right)\sin(\phi)-\left(1+\frac{\tilde{f}_0}{f_c}\right)\sin(\nu)\right\}\right)}{\sin^2\left(\frac{\pi}{2}\left\{\left(1+\frac{f_0}{f_c}\right)\sin(\phi)-\left(1+\frac{\tilde{f}_0}{f_c}\right)\sin(\nu)\right\}\right)} \tag{25}$$

$$\overset{(a)}{\approx} M^2\mathbb{F}_M^2\left(\left(1+\frac{f_0}{f_c}\right)\sin(\phi)-\left(1+\frac{\tilde{f}_0}{f_c}\right)\sin(\nu)\right), \tag{26}$$

where in (a), $\mathbb{F}_M(x)$ is the Fejér Kernel [33], which satisfies

$$\mathbb{F}_M(x) = \begin{cases} 1+o(M), & \text{if } x = 0, \\ 0, & \text{if } x \in \mathbb{Z}\backslash\{0\}, \\ o(M), & \text{if } x \in \mathbb{R}\backslash\mathbb{Z}. \end{cases} \tag{27}$$

Thus, to evaluate the angle at which the IRS vector has the largest response on frequency $\tilde{f}_0$, we set the argument of $\mathbb{F}_M(x)$ in (26) to 0, which upon simplification along with letting $\nu = \tilde{\phi}$ yields the desired result in (21). ■

From Lemma 1, we obtain the following two key insights:

1) Unless $\phi = 0°$, the IRS cannot focus all its energy in a single direction over the entire BW.
2) Hence, due to the B-SP effect, if the IRS is configured to reflect toward a nonzero cascaded angle ϕ at a particular frequency, it beamforms to a different direction at other frequencies within the BW. Lemma 1 formally establishes the conservation-of-energy argument discussed in Sec. II-D, namely, an IRS must necessarily steer its beam toward a different direction at frequencies other than the one to which it is tuned within the BW.

The directional response in Lemma 1 generalizes existing results in the literature. For example, [34] evaluates the reflection direction when the IRS is tuned to the center frequency ($f = 0$), whereas (21) evaluates the response when the IRS is tuned to an arbitrary frequency component within the BW.

B. Frequency Response of the IRS under B-SP effect

We note that Lemma (1) characterizes the directional response of an IRS, specifying the direction at which the IRS beamforms on a given frequency when it is actually tuned to reflect in a chosen direction on a different frequency. However, if the angular shift across two different frequencies exceeds the *Rayleigh resolution limit* of an array [12], the IRS effectively beamforms in multiple resolvable directions over the system bandwidth. In this view, we have the following result.

Lemma 2. *In an M-element IRS-aided wideband system with BW equal to W, the half-power beam width (HPBW) of the beam formed by the IRS towards the cascaded angle of ϕ on a frequency f_0 spans only a sub-band whose BW is given by*

$$W_\phi = \min\left\{\frac{4}{\pi}\sqrt{6\left(1-\frac{1}{\sqrt{2}}\right)}\cdot\frac{f_c}{M\sin(\phi)}, W\right\}. \tag{28}$$

Proof. When the IRS is set to align with the channel at a UE whose cascaded angle is ϕ on frequency f_0, the corresponding IRS configuration vector is given by (22). Then, the normalized IRS response on another frequency band centered at $\tilde{f}_0$ in the direction of ϕ can be evaluated as

$$\rho(\tilde{f}_0) \triangleq \frac{1}{M^2}\left|\boldsymbol{\theta}^{\text{opt}\,H}\mathbf{a}_M\left(\sin_{(p)}^{-1}\left\{\left(1+\frac{\tilde{f}_0}{f_c}\right)\sin(\phi)\right\}\right)\right|^2. \tag{29}$$

By simplifying (29) similar to the proof of Lemma 1, we get

$$\rho(\tilde{f}_0) = \left(\frac{\sin\left\{\frac{\pi M}{2}\left(\frac{f_0-\tilde{f}_0}{f_c}\right)\sin(\phi)\right\}}{M\sin\left\{\frac{\pi}{2}\left(\frac{f_0-\tilde{f}_0}{f_c}\right)\sin(\phi)\right\}}\right)^2, \tag{30}$$

which achieves the maximum when $f_0 = \tilde{f}_0$ or $\phi = 0$. Now, the frequency points corresponding to the HPBW of the beam formed by the IRS towards ϕ at f_0 can be obtained by setting $\rho(\tilde{f}_0) = 0.5$. Further, by using $|f_0 - \tilde{f}_0|/f_c \ll 1$ and $\sin(x) \approx$

x for $x \ll \pi$, from (30), we obtain a simplified relation for determining the sub-BW covering the HPBW of the beam as:

$$\operatorname{sinc}\left(\frac{M\sin(\phi)}{2}\left(\frac{f_0-\tilde{f}_0}{f_c}\right)\right)^2 \geq \frac{1}{2}. \tag{31}$$

Using the 1st order Taylor's approximation: $\operatorname{sinc}(x) \approx 1 - \frac{\pi^2 x^2}{6}$, which is tight in the regime of our interest, (31) simplifies to

$$\left|f_0-\tilde{f}_0\right| \leq \Delta f_\phi \triangleq \frac{2}{\pi}\sqrt{6\left(1-\frac{1}{\sqrt{2}}\right)}\cdot\frac{f_c}{M\sin(\phi)}, \tag{32}$$

From (32), we deduce that on a frequency component $\tilde{f}_0$ which is away from f_0 by a factor of at least Δf_ϕ, the IRS gain response in the direction of ϕ drops below the peak gain by at least a factor of $1/2$. Therefore, (32) characterizes the *effective one-sided bandwidth* for which appreciable array gain (corresponding to the HPBW) can be obtained from the IRS in the direction of ϕ. Since $\tilde{f}_0$ can lie on either side of the frequency component f_0, (28) can be obtained by setting $W_\phi = 2\Delta f_\phi$ and noting that W_ϕ cannot exceed W. ■

We now make the following remarks based on Lemma 2:

1) The BW W_ϕ corresponding to the HPBW of the beam formed by the IRS in direction ϕ is independent of the tuned frequency f_0. This indicates that the IRS exhibits a multi-directional response when it is tuned to any frequency within this BW. However, W_ϕ varies with ϕ because the impact of the B-SP depends on ϕ, as characterized in (17).
2) Even if the entire BW W is allotted to a single UE located at a physical angle of ϕ, the IRS provides the beamforming gain to this UE only over an effective BW given by (28).

C. The Multi-directional Beamforming

Based on the preceding discussions, when the IRS is tuned to reflect in direction ϕ_1 at a particular frequency, Lemma 1 characterizes its response across spatial directions, while Lemma 2 captures its response as a function of different frequency components within the BW. We now combine both these results and provide the main result of this section, which establishes the *multi-directional beamforming* property of the IRS under the B-SP effect.

Theorem 1. *Consider an M-element IRS-aided wideband system operating over a bandwidth of W around the carrier frequency f_c. Let $f_L \triangleq f_c - W/2$ denote the lower-edge frequency component of the band, and suppose the IRS is tuned to align with a cascaded angle ϕ_1 on the 1st sub-band, whose center frequency is*

$$f_1' \triangleq f_L + \frac{W_{\phi_1}}{2} = f_L + \frac{2}{\pi}\sqrt{6\left(1-\frac{1}{\sqrt{2}}\right)}\cdot\frac{f_c}{M\sin(\phi_1)}. \tag{33}$$

Now construct the set $\Phi_{\phi_1} \triangleq \{\phi_1, \ldots, \phi_{L_{\phi_1}}\}$ as follows:

$$\phi_\ell = \sin^{-1}_{(p)}\left\{\left(\frac{f_1'+f_c}{f_\ell'+f_c}\right)\sin(\phi_1)\right\}, \quad \ell = 2,\ldots,L_{\phi_1}, \tag{34}$$

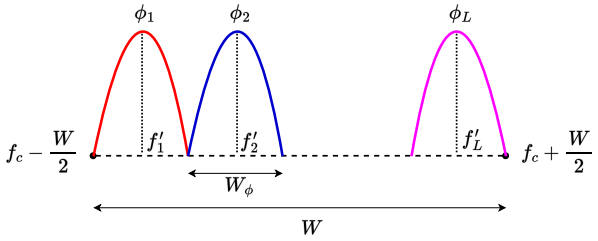

Fig. 3: Illustration of multi-directional beamforming with B-SP effect.

where the frequencies $\{f_\ell'\}_\ell$ are given by

$$f_\ell' = f_1' + (\ell-1)\sqrt{6\left(1-\frac{1}{\sqrt{2}}\right)}\frac{4f_c}{M\pi\sin(\phi_1)}, \tag{35}$$

for $\ell = 2,\ldots,L_{\phi_1}$ and L_{ϕ_1} is given by

$$L_{\phi_1} \triangleq \left\lceil \frac{MW\sin(\phi_1)}{1.7 f_c} \right\rceil. \tag{36}$$

Then, Φ_{ϕ_1} constitutes a set of resolvable angles, *i.e., $|\sin(\phi_i)-\sin(\phi_j)| \geq \mathcal{O}\left(\frac{1}{M}\right)$ for $i \neq j$, $i,j = 1,2,\ldots,L_{\phi_1}$, and such that the normalized correlation response of the IRS on the ℓth sub-band obeys*

$$\rho_{\ell,\ell'} \triangleq \frac{1}{M^2}\left|\mathbf{a}_M^H(\phi_\ell)\mathbf{a}_M(\phi_{\ell'})\right|^2 = \begin{cases} 1, & \text{if } \phi_{\ell'} = \phi_\ell, \\ \kappa, & \text{if } \phi_{\ell'} \neq \phi_\ell, \end{cases} \tag{37}$$

$\forall \ell' \in [L]$, where κ is a small number s.t. $\kappa \to 0$ as $M \to \infty$. Consequently, L_{ϕ_1} in (36) is the number of resolvable beams formed by the IRS when it is tuned to reflect in direction ϕ_1.

Proof. We first note that the frequencies $\{f_\ell'\}_{\ell=1}^{L_{\phi_1}}$ form an arithmetic progression with a common difference precisely equal to W_{ϕ_1}, as characterized in Lemma 2. According to Lemma 1, the angles $\{\phi_\ell\}_{\ell=1}^{L_{\phi_1}}$ defined in (34) correspond to the directions in which the IRS forms beams at frequencies f_ℓ', for $\ell = 2,\ldots,L_{\phi_1}$, when the IRS is actually configured to reflect toward the direction ϕ_1 at frequency f_1'.

Now, since W_{ϕ_1} quantifies the effective sub-BW over which the HPBW of the beam formed by the IRS extends, a frequency separation of at least W_{ϕ_1} between adjacent f_ℓ' ensures that the corresponding beam directions ϕ_ℓ are sufficiently separated in the angular domain, i.e., by $\mathcal{O}(1/M)$, which marks the Rayleigh resolution limit of the array. Consequently, these directions become *resolvable* by the IRS, and hence satisfy the resolvability condition given in (37).

Finally, the total number of resolvable beams formed by the IRS across the entire bandwidth when it is tuned to reflect toward ϕ_1 at $f = f_1'$ can be obtained by taking the ratio of the total bandwidth W to the effective sub-BW W_{ϕ_1} associated with the HPBW of a single beam. That is,

$$N_{\text{res}} = \frac{W}{W_{\phi_1}} = \frac{\pi}{4}\left(\sqrt{6\left(1-\frac{1}{\sqrt{2}}\right)}\right)^{-1}\cdot\frac{MW\sin(\phi_1)}{f_c}, \tag{38}$$

which, upon simplification and rounding up to the next largest integer, denoted by L_{ϕ_1}, gives the expression in (36). ■

From Theorem 1, we note that the number of resolvable beams formed by the IRS, L_ϕ, depends on the ratio MW/f_c, which is the term that controls the impact of the B-SP effect

in (17). When $MW/f_c > 1$, the number of beams formed increases linearly with this ratio. On the other hand, when the B-SP effect is negligible, $MW/f_c \ll 1$, and (36) yields $L_\phi = 1$, which is consistent with the existing studies on IRS-aided mmWave systems where the IRS beamforms to a given UE over the full BW [4], [5], [8]. To illustrate Theorem 2 in a practical case, consider a 5G NR compliant IRS-aided mmWave system with $M = 1024$, $W = 400$ MHz, $\phi = 90°$, and $f_c = 30$ GHz. Then, using (36), we get $L_\phi \approx 8$; which means the IRS can beamform up to 8 resolvable directions at the same time; each covering a BW equal to $400/8 = 50$ MHz and spanning the HPBW of a beam. Theorem 1 is pictorially illustrated in Fig. 3.

Capitalizing on the *multi-directional beamforming*, we next propose the *opportunistic OFDMA scheme* that exploits the B-SP effect of the IRS to maximize the system throughput.

IV. Exploiting Beam Split Via Opportunistic OFDMA

Since the B-SP effect causes a degradation in the achievable array gain over the BW if a single UE were to be scheduled over the entire BW, we propose to adopt an OFDMA framework wherein we schedule multiple UEs on different SCs. This fits naturally into the constraints imposed by the B-SP effect since no single UE is typically allotted the full BW. This motivates us to exploit the B-SP effect and enhance the throughput via an opportunistic OFDMA scheme.

To this end, we first solve for the optimal scheduler $\mathsf{SCH}(\cdot)$ in (P0) and then analyze the effectiveness of OFDMA in exploiting the B-SP effect to enhance the system performance.

A. The Opportunistic OFDMA for Exploiting the Beam-Split

From (P0), we note that the scheduler $\mathsf{SCH}(n,t)$ is decoupled across all N SCs and T time slots; thus it can be equivalently posed as solving NT independent optimization problems with the solution to $\mathsf{SCH}(n,t)$ depending on only the nth SC and tth time slot. Then, invoking the monotonicity property of the $\log(\cdot)$ function, the optimal scheduler that solves (P0) is one that maximizes the channel gain on each SC in every slot, i.e.,

$$\forall n \in [N], t \in [T],\ \mathsf{SCH}^{\text{opt}}(n,t) = \underset{k\in[K]}{\arg\max}\ |H(k,t,f_n)|^2, \tag{39}$$

and scheduler which implements (39) is referred to as the max-rate scheduler in the rest of this paper. We call the overall scheme *opportunistic OFDMA* because the system opportunistically schedules different UEs across the system BW and time to maximize the aggregate throughput, for a given IRS configuration (or sequence of configurations over time). However, note that different IRS configurations can lead to different scheduling outcomes and throughputs. Hence, we propose to randomly configure the IRS from a distribution that is aware of the channel model in every time slot [35]. Now, since the UEs are randomly located, we model the sine of the cascaded angle at different UEs as a uniform random variable:

$$\varphi_k^{\mathsf{C}} \triangleq \sin(\phi_k) \overset{d}{=} \tilde{\varphi}^{\mathsf{C}} \overset{\text{i.i.d.}}{\sim} \mathcal{U}[-1,1], \tag{40}$$

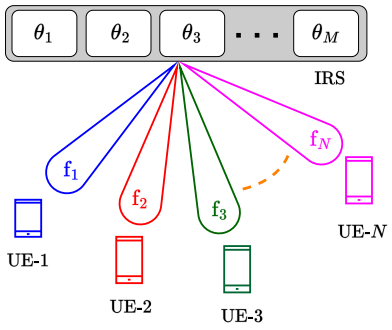

Fig. 4: Illustration of opportunistic OFDMA by exploiting the B-SP. Different colors indicate different frequency sub-bands.

where $\overset{d}{=}$ stands for "equal in distribution" [31]. Then, using [35, Sec. III.C], the random IRS configurations are sampled independently across slots as

$$\vartheta_m(t) = \pi(m-1)a(t),\ a(t) \overset{\text{i.i.d.}}{\sim} \mathcal{U}[-1,1],\ t \in [T]. \tag{41}$$

Note that the support of $a(t)$ in (41) represents the long-term cascaded angular range of the UEs' channels, as characterized in (40). If this cascaded angular range is known to lie within a different fixed interval, the corresponding long-term statistics can be acquired using the techniques in [36], and subsequently incorporated into the sampling distribution in (41). Further, [37] shows that randomly sampling the IRS phase angles according to (41) is throughput-optimal in a narrowband setting.[4] In this work, we continue to employ sampling the random phases as per (41) for the wideband setting as well, for three reasons: (a) each SC can still be treated as a narrowband channel at each UE, so sampling according to (41) remains valid; (b) the scheme which uses (41) is simple and requires no coordination with the BS; and (c) as we will show analytically in Theorem 2 and numerically in Sec. V, (41) is sufficient to achieve the full array gain across the entire operating BW.

Now, to illustrate how the B-SP effect can be exploited, using (41) in (19), we deduce that the channel gain at the kth UE on the nth SC at time slot t is given by

$$|H(k,t,f_n)|^2 = M^2 \left|\gamma_k^{\mathsf{C}}\right|^2 \text{sinc}^2\left(M\left(a(t) - \varphi_k^{\mathsf{C}}\left(1+\frac{f_n}{f_c}\right)\right)\right). \tag{42}$$

Then, for a given $a(t)$ at slot $t \in [T]$, on every SC $n \in [N]$, if there exists at least one UE-$k^*(t,n) \in [K]$ such that

$$a(t) - \varphi_{k^*(t,n)}^{\mathsf{C}}\left(1+\frac{f_n}{f_c}\right) \approx 0, \tag{43}$$

we can nearly achieve the maximum array gain of M^2 for every $t \in [T]$ and $n \in [N]$ by scheduling UE-$k^*(t,n)$. This way, in mmWave bands with large bandwidth, each SC can obtain the optimal array gain of M^2 in every time slot by exploiting multi-user diversity. This is illustrated in Fig. 4. In Sec. IV-B, we formally show that under the B-SP effect and with a large

[4] In the narrowband regime, a similar principle applies: when the IRS phases are randomly chosen, at least one UE will observe the IRS configuration that is nearly aligned with its BF direction. Then, scheduling that UE for data transmission yields the full IRS array gain. In [37], for the narrowband case, a variational functional optimization problem was solved to determine the optimal sampling distribution for the IRS phases.

number of UEs, at least one UE almost surely achieves the full array gain on every SC and time slot. Subsequently, we use this to analyze the achievable throughput of the above-described opportunistic OFDMA scheme in Sec. IV-D.

B. Eliminating B-SP via Multi-user Diversity Almost Surely

To facilitate further analysis, we define the *normalized array gain*, $G_M(k,t,n)$, achieved by UE-k on SC-n in slot t via an M-element IRS whose configurations are randomly chosen according to (41) as

$$G_M(k,t,n) \triangleq \frac{|H(k,t,f_n)|^2}{M^2\left|\gamma_k^{\mathsf{C}}\right|^2} \in [0,1], \tag{44}$$

with $G_M(k,t,n) = 1$ implying that a full-array gain is obtained. We then have the following theorem.

Theorem 2. *Consider an M-element IRS-aided wideband system with N subcarriers and K UEs whose cascaded angles via the IRS satisfy (40). Then, if the IRS phase configurations are randomly sampled as per (41), the normalized array gain defined in (44) satisfies: $\forall t \in [T]$,*

$$\lim_{K\to\infty} \mathsf{Pr}\left(\bigcap_{n=1}^{N}\bigcup_{k=1}^{K}\left\{\varphi_k^{\mathsf{C}} \in [-1,1] : G_M(k,t,n)=1\right\}\right) = 1. \tag{45}$$

As a result, the IRS almost surely provides the full array gain of M^2 (possibly at different UEs) over the entire BW, i.e.,

$$\mathsf{Pr}\Big(\Big\{\lim_{K\to\infty} \forall t\in[T], \forall n\in[N], \exists\, k^*(t,n)\in[K] : |H(k^*,t,f_n)|^2 = \left|\gamma_{k^*}^{\mathsf{C}}\right|^2 M^2\Big\}\Big) = 1, \tag{46}$$

where $k^*(t,n)$ denotes UE selected at slot t and SC n.

Proof. To prove (45), by using the continuity of probability, it suffices to show that

$$\mathsf{Pr}\left(\lim_{K\to\infty}\bigcap_{n=1}^{N}\bigcup_{k=1}^{K}\left\{\varphi_k^{\mathsf{C}} \in [-1,1] : G_M(k,t,n)=1\right\}\right) = 1, \tag{47}$$

which means to establish that as $K\to\infty$, the event $\mathcal{A}_K \triangleq \bigcap_{n=1}^{N}\bigcup_{k=1}^{K}\left\{\varphi_k^{\mathsf{C}}\in[-1,1]: G_M(k,t,n)=1\right\}$ occurs almost surely.

Now, by invoking a result from [38, Sec 7.2, Lemma $10(a)$], a necessary and sufficient condition for (47) to hold true can be rewritten as: $\forall \epsilon > 0$,

$$\mathsf{Pr}\left(\lim_{K\to\infty}\sup\bigcup_{n=1}^{N}\bigcap_{k=1}^{K}\left\{\varphi_k^{\mathsf{C}} : |G_M(k,t,n)-1| > \epsilon\right\}\right) = 0. \tag{48}$$

Define the event $\mathcal{A}_K^{\epsilon} \triangleq \bigcap_{n=1}^{N}\bigcup_{k=1}^{K}\left\{\varphi_k^{\mathsf{C}} : |G_M(k,t,n)-1| \le \epsilon\right\}$. Then the probability of its complementary event is given by

$$\begin{aligned}\mathsf{Pr}\left((\mathcal{A}_K^{\epsilon})^c\right) &= \mathsf{Pr}\left(\bigcup_{n=1}^{N}\bigcap_{k=1}^{K}\left\{\varphi_k^{\mathsf{C}} : |G_M(k,t,n)-1| > \epsilon\right\}\right)\\ &\overset{(a)}{\le} \sum_{n=1}^{N}\mathsf{Pr}\left(\bigcap_{k=1}^{K}\left\{\varphi_k^{\mathsf{C}} : |G_M(k,t,n)-1| > \epsilon\right\}\right)\\ &\overset{(b)}{=} \sum_{n=1}^{N}\prod_{k=1}^{K}\mathsf{Pr}\left(\left\{\varphi_k^{\mathsf{C}} : |G_M(k,t,n)-1| > \epsilon\right\}\right), \end{aligned} \tag{49}$$

where in (a), we used the union-bound over the events associated with all the N-SCs, and in (b), we used the fact that the events $\mathcal{A}_K^{\epsilon,k,n} \triangleq \left\{\varphi_k^{\mathsf{C}} : |G_M(k,t,n)-1| \le \epsilon\right\}$ (and their complements) are independent across $k\in[K]$. In the sequel, we characterize the probability of $\mathcal{B}_K^{\epsilon,k,n} \triangleq \left(\mathcal{A}_K^{\epsilon,k,n}\right)^c$, the complementary event of $\mathcal{A}_K^{\epsilon,k,n}$. To this end, note that

$$\begin{aligned}\mathcal{B}_K^{\epsilon,k,n} &\overset{(c)}{=} \left\{\varphi_k^{\mathsf{C}} : \mathrm{sinc}^2\left(M\left(a(t) - \left(1+\frac{f_n}{f_c}\right)\varphi_k^{\mathsf{C}}\right)\right) \le 1-\epsilon\right\}\\ &\overset{(d)}{=} \left\{\varphi_k^{\mathsf{C}} \in [-1,1] : \left|a(t) - \left(1+\frac{f_n}{f_c}\right)\varphi_k^{\mathsf{C}}\right| \ge \frac{\sqrt{3\epsilon}}{\pi M}\right\}\\ &= \left\{\varphi_k^{\mathsf{C}} \in [-1,1] : \varphi_k^{\mathsf{C}} \notin \left(a(t) \pm \frac{\sqrt{3\epsilon}}{\pi M}\right) \Big/ \left(1+\frac{f_n}{f_c}\right)\right\}, \end{aligned} \tag{50}$$

where in (c), we used the expressions in (44) followed by (42), and in (d), we used the Taylor's approximation: $\mathrm{sinc}^2(x) \approx 1-\pi^2x^2/3$, which is tight under the regime of interest to us. Now, since $\varphi_k^{\mathsf{C}} \sim \mathcal{U}[-1,1]$, we can show that

$$\mathsf{Pr}\left(\mathcal{B}_K^{\epsilon,k,n}\right) = 1 - \frac{\sqrt{3\epsilon}}{\pi M\left(1+\frac{f_n}{f_c}\right)} \overset{(e)}{\le} 1 - \frac{\sqrt{3\epsilon}}{\pi M\left(1+\frac{W}{2f_c}\right)}, \tag{51}$$

where we noted that $|f_n| \le W/2,\ n\in[N]$. Using (51) in (49), we obtain

$$\mathsf{Pr}\left((\mathcal{A}_K^{\epsilon})^c\right) \le N\left(1 - \frac{\sqrt{3\epsilon}}{\pi M\left(1+\frac{W}{2f_c}\right)}\right)^K. \tag{52}$$

Now, consider the infinite sum:

$$\begin{aligned}P_{\infty}^{\epsilon} &\triangleq \sum_{K=1}^{\infty}\mathsf{Pr}\left((\mathcal{A}_K^{\epsilon})^c\right) \overset{(e)}{\le} N\sum_{K=1}^{\infty}\left(1 - \frac{\sqrt{3\epsilon}}{\pi M\left(1+\frac{W}{2f_c}\right)}\right)^K\\ &\overset{(g)}{=} P_{\infty}^{\epsilon,\mathrm{U}} \triangleq \frac{\pi NM\left(1+\frac{W}{2f_c}\right)}{\sqrt{3\epsilon}}, \end{aligned} \tag{53}$$

where in (e), we used (52), and in (g), we used the formula of an infinite geometric series. Now since we have $\forall\epsilon>0$, $0 \le P_{\infty}^{\epsilon} \le P_{\infty}^{\epsilon,\mathrm{U}} < \infty$, by using Borel-Cantelli Lemma [38, Sec 7.3, Theorem $10(a)$], we deduce that

$$\forall \epsilon > 0, \quad \mathsf{Pr}\left(\lim_{K\to\infty}\sup\left(\mathcal{A}_K^{\epsilon}\right)^c\right) = 0, \tag{54}$$

which proves the statement in (48). Consequently, we have

$$\mathsf{Pr}\left(\lim_{K\to\infty}\mathcal{A}_K\right) = \mathsf{Pr}\left(\lim_{K\to\infty}\bigcap_{n=1}^{N}\bigcup_{k=1}^{K}\left\{\varphi_k^{\mathsf{C}} : G_M(k,t,n)=1\right\}\right) = 1, \tag{55}$$

which completes the proof of (45). Note that this holds for all time slots $t\in[T]$. Finally, using the sequential definition of the almost sure convergence of random variables in (47), the result in (46) follows. Importantly, (46) rigorously shows that, in every slot and SC, despite exhibiting a B-SP, the IRS will

provide a full-array gain to at least one UE when the number of UEs is large. This completes the proof. ■

Theorem 2 establishes that, by positively exploiting the B-SP effect, on every SC and every time slot, the channel gain for at least one UE will achieve the full IRS array gain of M^2, even when UEs are randomly located. In retrospect, this result stems from the *multi-directional beamforming* capability induced by the B-SP effect, as characterized in Theorem 1, which allows the IRS to simultaneously form distinct beams over different frequency components.

Remark 3 (On the number of subcarriers)**.** *Theorem 2 shows that, across all frequency components within the total BW, at least one UE attains the full array gain. However, since practical OFDM systems employ a finite number of SCs, the smallest frequency unit that can be allotted has a BW equal to the SC spacing. In our analysis, we assume that the SC spacing is sufficiently small for the variation in channel gain due to residual B-SP/B-SQ effects within each SC to be negligible, allowing the channel gain to be treated as approximately constant within an SC. For instance, by requiring that the gain over the entire SC remains at least a $(1-\epsilon)$ fraction (for some small $\epsilon \in (0,1)$) of the gain at its center frequency in (17), one can determine an appropriate number of SCs for a near-flat response within an SC.*

C. How Many UEs are Sufficient in Practice?

In the previous section, we theoretically proved that we can obtain *full array gain* from the IRS as $K \to \infty$. A related question of practical interest is: *How many UEs are sufficient for the near-beamforming condition to hold with high probability?* We answer this next.

Proposition 1. *Let $\epsilon, \delta \in (0,1)$ be small positive constants. Consider an IRS-aided wideband system with M reflecting elements, N subcarriers spanning a total bandwidth of W around a carrier frequency of f_c. Under the setting of Theorem 2, if the number of UEs, K, satisfies*

$$K \geq K^* \triangleq -\frac{\ln\left(\frac{N}{\delta}\right)}{\ln\left(1-\frac{\sqrt{3\epsilon}}{\pi M\left(1+(W/2f_c)\right)}\right)}, \tag{56}$$

then, with probability at least $1-\delta$, there exists at least one UE on every subcarrier that achieves an array gain of $(1-\epsilon)M^2$.

Proof. We first define the "$(1-\epsilon)M^2$ *success event*":

$$\mathcal{E}^{\epsilon}_{k,n} \triangleq \left\{\varphi^{\mathsf{C}}_k \in [-1,1] : G_M(k,t,n) \geq 1-\epsilon\right\}, \tag{57}$$

that denotes the event that the array gain via the IRS on SC-n at UE-k is at least $(1-\epsilon)M^2$ at some time t. Since the success of the overall scheme is determined by obtaining a near-optimal array gain for at least one UE, we define the *overall probability of $(1-\epsilon)M^2$ success event* as

$$P^{\epsilon}_{\text{succ}} \triangleq \mathsf{Pr}\left(\bigcap_{n=1}^{N}\bigcup_{k=1}^{K}\mathcal{E}^{\epsilon}_{k,n}\right). \tag{58}$$

Note that the above probability is exactly the probability of the event, $\mathcal{A}^{\epsilon}_K$ defined after (48) in the proof of Theorem 2. Thus, by directly using the expression given in (52), we get

$$P^{\epsilon}_{\text{succ}} \geq 1 - N\left(1-\frac{\sqrt{3\epsilon}}{\pi M\left(1+\frac{W}{2f_c}\right)}\right)^{K}. \tag{59}$$

Finally, by substituting for $P^{\epsilon}_{\text{succ}} = 1-\delta$, and upon rearranging the terms above, we obtain the desired expression in (56). ■

Based on Proposition 1, to effectively exploit the B-SP effect and obtain full array gain over the BW, the minimum number of UEs, K^*, scales as follows:

1) As δ decreases, we target a higher probability of success. For this, the number of UEs scales as $\mathcal{O}(\ln(1/\delta))$. In particular, as $\delta \to 0$, $K^* \to \infty$, consistent with Theorem 2.
2) Reducing ϵ corresponds to a lower tolerance for degradation in the achievable array gain of M^2. This, in turn, requires K^* to scale roughly as $\mathcal{O}(\sqrt{1/\epsilon})$ so that at least one UE aligns closely with the IRS beam direction. This is again consistent with Theorem 2. (see also [39, Prop. 2].)
3) As either M (the number of IRS elements) or W (system BW) increases, the B-SP effect becomes more pronounced, leading to a larger number of IRS-formed beams, in accordance with Theorem 1. Consequently, more UEs are needed so that at least one can be scheduled for each distinct beam formed by the IRS. In fact, when $MW/2f_c \gg 1$, we can approximate $-\ln(1-x) \approx x$ in the denominator of (56), and observe that $K^* \sim \Omega\left(MW/f_c\right) \sim \Omega(L_{90^\circ})$, where L_{90° is the number of resolvable beams formed by the IRS as given in (36) with $\phi = 90^\circ$. This is because the system requires at least as many UEs as the maximum number of resolvable beams formed by the IRS via the B-SP effect.

We note that the requirement on the number of UEs in our design aligns well with current wireless system practices and does not represent an additional requirement specific to our study. Notably, one of the key wireless use-cases is massive machine-type communications (MMTC), which is envisioned to support 10^6 users per km^2 [40].[5]

D. Achievable Throughput

Having established that the B-SP effect enables full array gain at different UEs across the BW, we now derive the achievable throughput under the opportunistic OFDMA scheme described in Sec. IV-A when $\bar{\alpha}$ is modeled as a deterministic channel with $|\bar{\alpha}|^2 = \rho_1$ [37], while $\bar{\beta}_k \sim \mathcal{CN}(0, \rho_{2,k})$ represents a Rayleigh fading channel. Here, ρ_1 and $\rho_{2,k}$ denote the respective path losses. For analytical tractability, we assume that all UEs experience identical path loss, similar to [41].

Theorem 3. *The system throughput, denoted by $R^{(K)}$, of an OFDMA scheme in a randomly configured (as per (41)) large IRS-aided wideband system using a max-rate scheduler (as per (39)) and equal power allocation across all SCs satisfies*

$$\lim_{K\to\infty}\left(R^{(K)} - \mathcal{O}\left\{W\log_2\left(1+\frac{\rho P}{N\sigma^2}N_t M^2 \ln K\right)\right\}\right) = 0,$$

[5]For example, in a small cell of radius 100 m and a user activity rate of 10%, there will be a few hundred active UEs at a given time; roughly the scale of the number of UEs we consider in this work.

where $\rho \triangleq \rho_1\rho_2$ is the cascaded path loss across the UEs ($\rho_2 = \rho_{2,k}, \forall k$), and other symbols are as defined earlier.

Proof. Note that the throughput under equal power allocation across all SCs (from (P0)) with a max-rate scheduler is

$$R_{\text{MR}} \triangleq \frac{1}{T}\sum_{t=1}^{T}\sum_{n=1}^{N}\frac{W}{N}\log_2\left(1+\frac{P}{N_tN\sigma^2}\max_{k\in[K]}|H(k,t,f_n)|^2\right). \tag{60}$$

Now, considering that the channels are jointly stationary and ergodic and using Jensen's approximation over the $\log_2(\cdot)$ function, we simplify (60) as $R_{\text{MR}} \approx$

$$R^{(K)} \triangleq \sum_{n=1}^{N}\frac{W}{N}\log_2\left(1+\frac{P}{N_tN\sigma^2}\mathbb{E}\left[\max_{k\in[K]}|H(k,t,f_n)|^2\right]\right). \tag{61}$$

To characterize the expectation in (61), using (42), we can show that $|H(k,t,f_n)|^2=$

$$M^2N_t^2\rho_1\rho_2\left|\tilde{\gamma}_k^{\mathsf{C}}\right|^2\text{sinc}^2\left(M\left(a(t)-\varphi_k^{\mathsf{C}}\left(1+\frac{f_n}{f_c}\right)\right)\right), \tag{62}$$

with $\tilde{\gamma}_k^{\mathsf{C}} \triangleq \gamma_k^{\mathsf{C}}/\sqrt{\rho_1\rho_2}N_t$, so that $\tilde{\gamma}_k^{\mathsf{C}} \overset{\text{i.i.d.}}{\sim} \mathcal{CN}(0,1)$. From Theorem 2, as $K\to\infty$, we know that on every SC, at least one UE will be in near-beamforming configuration. Then, the maximum of the terms given in (62) is the maximum over the channel gains among those UEs for whom the IRS phases are in near-beamforming configurations (i.e., for those UEs for whom $|H(k,t,f_n)|^2 = M^2N_t^2\rho_1\rho_2\left|\tilde{\gamma}_k^{\mathsf{C}}\right|^2$). Thus, we have

$$\mathbb{E}\left[\max_{k\in[K]}|H(k,t,f_n)|^2\right] \approx M^2N_t^2\rho_1\rho_2\mathbb{E}\left[\max_{k\in[K]}\left|\tilde{\gamma}_k^{\mathsf{C}}\right|^2\right]+\mathcal{O}(1). \tag{63}$$

Now, to characterize the expected value of the order statistic in (63), we first recognize that $\left|\tilde{\gamma}_k^{\mathsf{C}}\right|^2$ is an exponential random variable with mean 1, and then by using results from extreme value theory [35, Lemma 3], we can show that, for large K, $\max_{k\in[K]}\left|\tilde{\gamma}_k^{\mathsf{C}}\right|^2$ grows as l_K, where $F(l_K) = 1-\frac{1}{K}$ with $F(z) = 1-e^{-z}$, which is the cumulative distribution function of a unit mean exponential random variable. Then, using the value of $l_K = \ln K$ in (63), and substituting the resulting expression in (61), we can show that the throughput scales as

$$R^{(K)} \lesssim W\log_2\left(1+\frac{\rho P}{N\sigma^2}N_tM^2\ln K\right), \tag{64}$$

which is restated in the statement of the theorem. ∎

Theorem 3 establishes that, by exploiting the B-SP effect at the IRS, a channel gain of $\mathcal{O}(M^2)$ can be achieved on all SCs. Moreover, in fading channels, an additional SNR gain that scales as $\mathcal{O}(\ln K)$ arises from multi-user diversity, analogous to the scaling obtained in sub-6 GHz systems in [35, Theorem 4], on top of the array gain from the BS antenna array, which scales linearly with N_t. Thus, by utilizing opportunistic scheduling, the system can achieve a throughput comparable to that of a network that is effectively transparent to the B-SP phenomenon at the IRS.

Remark 4 (Tuning of fairness)**.** *In general, opportunistic scheduling schemes with the max-rate metric do not ensure fairness in the scheduling of UEs. Fairness can be ensured by employing, e.g., a proportional-fair (PF) scheduler [42], which provides a tunable trade-off between throughput and fairness in UE scheduling. This paper focuses on max-rate scheduling to highlight the idea of exploiting the B-SP effect; however, the analysis can be extended to other scheduling strategies as well. For e.g., our prior work [35] investigates PF scheduling with randomized IRS in a narrowband setup.*

E. Exploiting Beam-Split Effects in Near-Field Systems

Until the previous subsection, we assumed that all nodes lie in the far-field of both the BS and IRS arrays, implying that the transmitted and received wavefronts at these arrays can be well approximated as planar. To a first-order approximation, this assumption holds provided that (i) the distance between the IRS and the UEs exceeds the Rayleigh distance of the IRS, $d_{\text{Rayleigh}}^{\text{IRS}}$, and (ii) the distance between the BS and IRS exceeds both the Rayleigh distance of the IRS, $d_{\text{Rayleigh}}^{\text{IRS}}$, and that of the BS, $d_{\text{Rayleigh}}^{\text{BS}}$. The Rayleigh distance of an array is defined as

$$d_{\text{Rayleigh}}^{\text{X}} = 2D_{\text{X}}^2\big/\lambda_c, \quad \text{X}\in\{\text{BS},\text{IRS}\}, \tag{65}$$

where D_{BS} and D_{IRS} denote the aperture lengths of the BS and IRS arrays, respectively, and λ_c is the carrier wavelength.

When the above conditions are not satisfied, the impinging and reflected signals exhibit spherical wavefronts, and the system operates in the radiative near-field regime. In the following, we discuss how the proposed opportunistic OFDMA can be extended to account for such near-field effects. Since the IRS typically has a much larger aperture than the BS (for reasons discussed in Sec. I-A), we focus on the practically relevant scenario where both the BS and the UEs lie in the near-field of the IRS. The IRS itself, however, may be located in either the far-field or near-field of the BS array [43].

In the near-field regime, the delay components of the IRS-assisted channel in (5) and (6) must include second-order distance-dependent terms to account for the spherical wavefront of the signal impinging on the IRS. As before, let ψ and ω_k denote the DoA and DoD at the IRS from the BS and UE-k, respectively, and let $r_1 \le d_{\text{Rayleigh}}^{\text{IRS}}$ and $r_{2,k} \le d_{\text{Rayleigh}}^{\text{IRS}}$ denote the distances from the IRS to the BS and UE-k, respectively. Using the near-field channel model in [44], and assuming an appropriate timing-advance-based precoder at the BS, similar to that in Sec. II-C, the overall channel gain at UE-k on baseband frequency f via the IRS can be simplified as in (66)-(67). In step (a), we define the cascaded angle at UE-k as $\phi_k \triangleq \sin^{-1}_{(p)}(\sin(\psi)-\sin(\omega_k))$, set $d_{\text{IRS}} = \lambda_c/2$, and introduce the *distance-ring* parameters $\Upsilon_1 \triangleq \frac{\cos^2(\psi)}{2r_1}$, and $\Upsilon_{2,k} \triangleq \frac{\cos^2(\omega_k)}{2r_{2,k}}$. To illustrate the B-SP effect in the near-field regime, we first tune the IRS to coherently focus energy toward UE-k at the center frequency, yielding the IRS phase configuration:

$$\vartheta_m = \pi\left(-(m-1)\sin(\phi_k)+(m-1)^2\frac{\lambda_c}{2}(\Upsilon_1+\Upsilon_{2,k})\right). \tag{68}$$

Letting $\Upsilon_k^{\mathsf{C}} \triangleq \Upsilon_1+\Upsilon_{2,k}$ and substituting (68) into (67), the resulting channel gain is $|H_k(f)|^2=$

$$\left|\gamma_k^{\mathsf{C}}\right|^2\left|\sum\nolimits_{m=1}^{M}e^{j\pi\frac{f}{f_c}\left\{(m-1)\sin(\phi_k)-(m-1)^2\frac{\lambda_c}{2}\Upsilon_k^{\mathsf{C}}\right\}}\right|^2. \tag{69}$$

$$|H_k(f)|^2 = \left|\gamma_k^{\mathsf{C}}\right|^2 \left| \sum_{m=1}^{N} e^{-j2\pi(f+f_c)\left\{-\frac{d_{\text{IRS}}}{c}(m-1)\{\sin(\psi)-\sin(\omega_k)\}+\frac{(m-1)^2 d_{\text{IRS}}^2}{c}\left\{\frac{\cos^2(\psi)}{2r_1}-\frac{\cos^2(\omega_k)}{2r_{2,k}}\right\}\right\}} \times e^{j\vartheta_m} \right|^2 \tag{66}$$

$$\overset{(a)}{=} \left|\gamma_k^{\mathsf{C}}\right|^2 \left| \sum_{m=1}^{M} e^{-j\pi\left(1+\frac{f}{f_c}\right)\left\{-(m-1)\sin(\phi_k)+(m-1)^2\frac{\lambda_c}{2}(\Upsilon_1+\Upsilon_{2,k})\right\}} \times e^{j\vartheta_m} \right|^2 \tag{67}$$

It is evident from (69) that, unless $f = 0$ or $\phi_k = \Upsilon_k^{\mathsf{C}} = 0$, the above summation does not attain its peak value of M. This condition is analogous to that in the far-field case in (17), with the additional requirement that the distance-dependent parameter Υ_k^{C} must be 0. In particular, as $r_1, r_{2,k} \to \infty$, we have $\Upsilon_k^{\mathsf{C}} \to 0$, which corresponds to the far-field regime, and the condition for achieving the full array gain reduces to that in (17). Evaluating (69) in closed form is mathematically involved and requires Fresnel integrals; for e.g., see [45].

Motivated by this observation, instead of tuning the IRS to a particular UE over the entire BW, similar to (41), in the near-field, we randomly sample the IRS phase configuration as $\vartheta_m(t) =$

$$\pi\left(-(m-1)a(t)+(m-1)^2\frac{\lambda_c}{2}\left(\Upsilon_1+\frac{1-a^2(t)}{2b(t)}\right)\right), \tag{70}$$

where $a(t) \overset{\text{i.i.d.}}{\sim} \mathcal{U}[-1,1]$ and $b(t) \overset{\text{i.i.d.}}{\sim} \mathcal{U}[0, d_{\text{Rayleigh}}^{\text{IRS}}]$, $\forall t \in [T]$. [6] Then, for a given realization of $(a(t), b(t))$, at time t and on SC n, if there exists a UE-$k^*(t,n) \in [K]$ such that

$$a(t) - \sin(\phi_{k^*(t,n)})\left(1+\frac{f_n}{f_c}\right) \approx 0, \text{ and,} \tag{71}$$

$$\frac{1-a^2(t)}{2b(t)} - \Upsilon_{2,k^*(t,n)}\left(1+\frac{f_n}{f_c}\right) \approx 0, \tag{72}$$

then the full IRS array gain of M^2 can be nearly achieved on that SC by scheduling UE-$k^*(t,n)$. These conditions indicate that, to exploit the B-SP effect, on each SC, a UE whose angle-distance pair aligns most favorably with the randomized IRS response will be scheduled. Consequently, through such opportunistic OFDMA, the IRS provides full *beamfocusing* gain of M^2 on every SC. See Fig. 5 for an illustration.

Similar to Theorem 2, one can show that the conditions in (71) and (72) occur with probability one as $K \to \infty$; we omit the details due to space constraints.

F. Signal Processing Complexity in the Implementation

We now discuss several signal processing merits related to the practical implementation of the proposed opportunistic OFDMA scheme with randomly configured IRS phases.

1) **Low-overhead feedback for opportunistic scheduling:** In our proposed scheme, to implement the opportunistic scheduler, the BS should know the index of the UE with the best channel gain on each SC. This can be obtained using efficient, low-complexity feedback schemes on an SC-by-SC basis. For e.g., the timer-feedback mechanism in [46] uses a single pilot, and on every SC, the UE with the best channel quality feeds back to the BS earlier than other UEs. In this way, the BS acquires the necessary scheduling information on every SC, and its overheads do not scale with the number of UEs in the system.
2) **IRS and control overheads:** Traditional IRS optimization frameworks incur substantial overhead due to (i) estimating the cascaded BS-IRS-UE channel for every UE, (ii) running a non-convex optimization to compute the IRS phases, and (iii) transporting the optimized phases to the IRS controller. The overhead of each step scales at least as $\mathcal{O}(M)$ per scheduling interval. In contrast, our approach eliminates all these overheads: the IRS draws its phases randomly and locally, and the BS only requires a short feedback signal from the "winning" UE on each SC.
3) **Computational cost at the BS:** The BS does not perform any IRS-related optimization or high-dimensional channel estimation; its sole task is to identify, on each SC, which UE's feedback (e.g., timer expiration) arrives first and schedule that UE for data transmission. This is the complexity of standard OFDMA opportunistic scheduling even in the absence of an IRS. Hence, our scheme offers a low-complexity method for integrating an IRS in real-time systems. However, if the long-term statistics of the UEs' channels change, it requires an update of the sampling distribution; though, this happens occasionally.

In summary, the proposed scheme achieves full IRS array gain with low hardware complexity, minimal signaling overhead, and only coarse synchronization with the BS, making it practical for wideband IRS-aided mmWave systems.

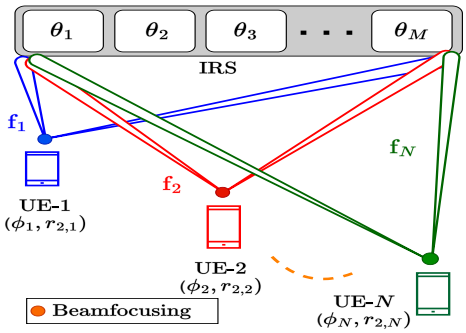

Fig. 5: Exploiting B-SP effect in near-field.

V. Numerical Results

We numerically illustrate the throughput enhancement obtained by exploiting the B-SP effect in the mmWave bands via OFDMA using Monte Carlo simulations. Unless stated otherwise, all the simulation parameters are listed in Table I, selected according to [29], [47]. The path loss is modeled as

[6] In (70), the parameter Υ_1, which depends on the fixed BS-IRS geometry, is assumed known at the IRS and can be readily obtained in practice.

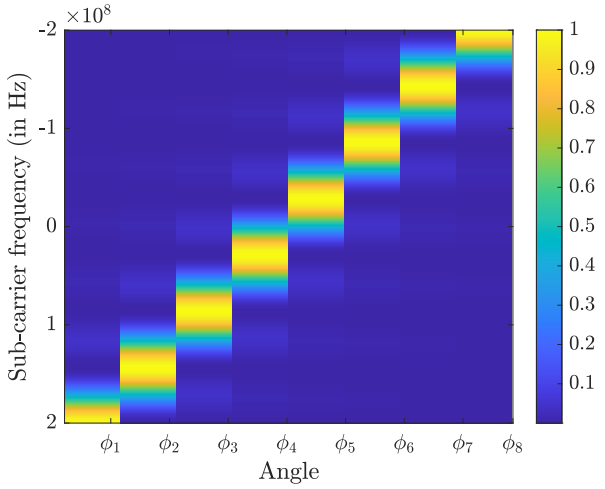

(a) Heat map of the normalized array gain as a function of angle & frequency.

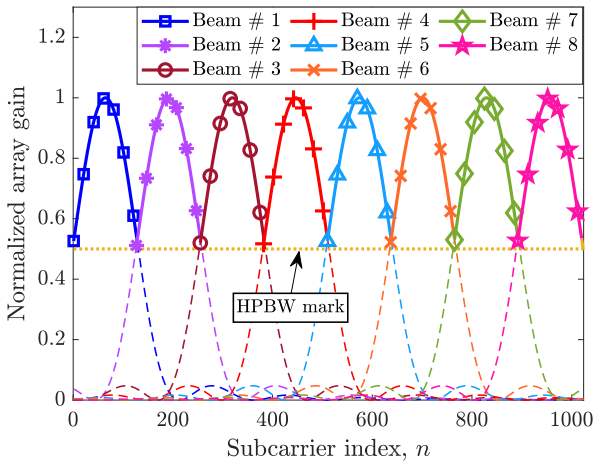

(b) Envelop of the normalized array gain vs. SC frequency.

Fig. 6: Illustrating the multi-directional beamforming property when the IRS is tuned to $\phi = 90°$.

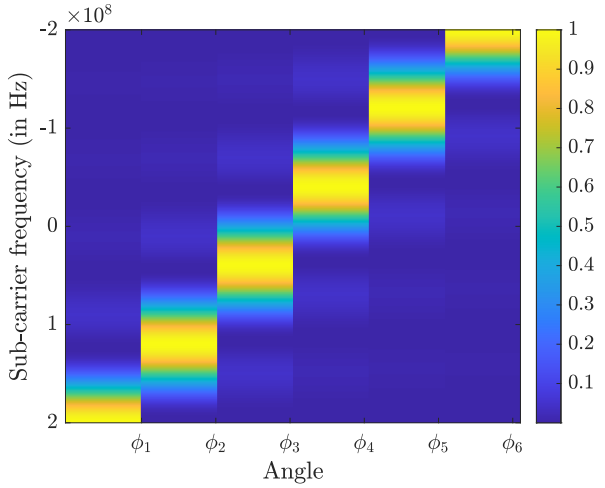

(a) Heat map of the normalized array gain as a function of angle & frequency.

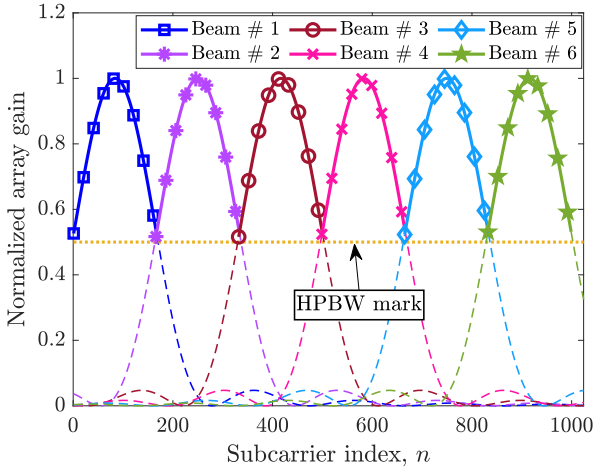

(b) Envelop of the normalized array gain vs. SC frequency.

Fig. 7: Illustrating the multi-directional beamforming property when the IRS is tuned to $\phi = 50°$.

TABLE I: Simulation configurations.

Simulation parameter	Value
The number of BS antennas, N_t	64
The number of IRS elements, M	1024
The number of UEs, K	Varied from 1 to 10^4
Carrier frequency, f_c	30 GHz
Bandwidth, W	400 MHz
The number of SCs, N	1024
BS and IRS locations	$(0, 0)$ and $(100, 100)$, resp.
UE angle distribution, $\mathcal{R}$	$\mathcal{U}[50°, 90°]$
Transmit power, P	40 dBm
Noise variance at UE, σ^2	-120 dBm
Path loss exponent in BS-IRS link	2
Path loss exponent in IRS-UE link	2.2

$\mathsf{PL} = C_0 \left(d_0/d_{\text{link}}\right)^{\mu_{\text{link}}}$, where $C_0 = -60$ dB is the path loss at the reference distance of $d_0 = 1$ m, d_{link} is the link distance, and μ_{link} denotes the link path loss exponent.

A. Multi-Directional Property of the IRS under B-SP Effect

We first illustrate the multi-directional beamforming property of the IRS given in Theorem 1 under the B-SP effect.

In Fig. 6a, we present a heatmap of the normalized array gain as a function of angle and subcarrier frequency in the baseband domain. The values along the x-axis represent the angles specified in Theorem 1. From the heatmap, we observe that the IRS indeed reflects its energy in different directions as we sweep across the BW.

In Fig. 6b, we plot the normalized gain of the IRS as a function of SC frequency when it is configured to reflect toward $\phi = 90°$ at the center frequency, $f_n = 0$. Each curve, labeled Beam #1 to #8, represents the IRS response in a specific direction, corresponding to the angles derived in Lemma 1 for $f_n = 0$, $\phi = 90°$, and $\tilde{f}_0$ set to $\{f'_\ell\}_{\ell=1}^{L_\phi}$ determined using (35) from Theorem 1. The figure shows that the IRS achieves full array gain in different *resolvable* directions (i.e., the angles which do not lie within the HPBW of the beam formed on other angles) over distinct frequency bands centered around the frequencies given by (35), thereby confirming that the IRS exhibits multi-directional beamforming simultaneously across multiple contiguous and non-overlapping sub-bands. Furthermore, the number of resolvable beams formed across the system BW is 8 in this figure, which matches the theoretical value derived in Theorem 1.

In Fig. 7a and Fig. 7b, we repeat the previous experiment with the IRS now configured to reflect toward $\phi = 50°$ at the center frequency $f_n = 0$. Similar to the earlier case, we

observe that the IRS provides beamforming gain in multiple directions across different SCs, showing its ability to form several resolvable beams over the BW. However, unlike Fig. 6a and Fig. 6b, the number of beams formed across the system bandwidth is smaller for $\phi = 50°$ compared to $\phi = 90°$. This reduction arises because, as the reflection angle moves away from $90°$, the signal experiences a relatively smaller SDS through the IRS, as described in (11). Consequently, the SWE and the resulting B-SP phenomenon become less pronounced. According to Theorem 1, a weaker B-SP leads to fewer resolvable beams. Thus, this experiment highlights that both the beamforming capability of the IRS and the number of beams it can form depend on the angle at which it is configured to reflect at $f_n = 0$.

B. Performance of Opportunistic OFDMA under B-SP Effect

Leveraging the multi-directional beamforming capability of the IRS, we now turn our attention to demonstrating the performance of the proposed opportunistic OFDMA scheme.

Figure 8 depicts the normalized array gain, averaged over all UEs, as a function of the baseband SC frequency for the following cases (as indicated in the figure legend):

1) **Opportunistic OFDMA with fading:** The IRS is randomly configured as per (41), and UEs are scheduled using a max-rate OFDMA scheduler with random channel fading.
2) **Opportunistic OFDMA without fading:** The IRS is randomly configured and max-rate scheduling of UEs is employed without channel fading, i.e., γ_k^{C} is deterministic.
3) **Benchmarking with TTD-based performance:** A genie-aided benchmark using a TTD-enabled IRS with round-robin (RR) scheduling across the entire BW.
4) **Round-robin SU-OFDM without fading: UPA/ULA:** A single UE is scheduled per time slot over the full BW using RR scheduling, and the IRS is optimized for this UE at the center frequency $f_n = 0$, with the IRS implemented as (a) an $M/4 \times 4$ UPA and (b) a ULA.
5) **Max-min beamforming, RR SU-OFDM:** A single UE is scheduled per time slot across the full BW in an RR fashion, and the IRS phases are chosen to maximize the minimum channel gain over the BW [48], [49].

First, under RR scheduling, the array gain attains $\mathcal{O}(M^2)$ only at the center SC $f_n = 0$ for both ULA- and UPA-based IRSs, and degrades significantly at other SCs due to the B-SP effect. This confirms that phase-shifter-based IRSs are inherently inadequate for wideband beamforming. Although an $M/4 \times 4$ UPA-based IRS outperforms its ULA counterpart with the same number of elements M due to a reduced B-SP severity, it does not fully eliminate the performance loss. In contrast, the scheme considered in this paper consistently outperforms these baselines by effectively exploiting the B-SP effect through multi-user diversity. When multiple UEs are multiplexed using OFDMA, the average channel gain becomes more uniform across the BW. In the absence of fading, the gain remains flat at its peak value of $\mathcal{O}(M^2)$. With channel fading, the average gain further increases due to multi-user diversity and exceeds the peak gain achieved under RR scheduling. We also benchmark our approach against a genie-aided TTD-based IRS, as discussed in Sec. I-B. The proposed scheme

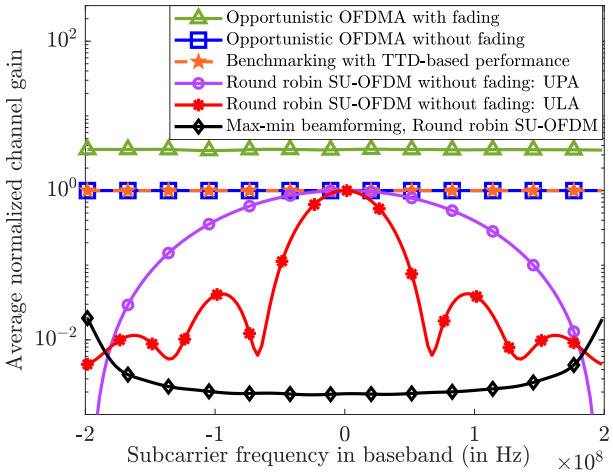

Fig. 8: Avg. normalized array gain with $K = 1000$.

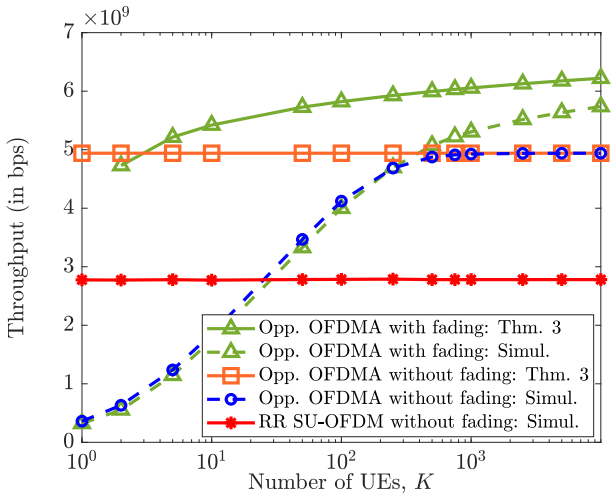

Fig. 9: Throughput vs. No. of UEs, K.

outperforms this benchmark also while relying on a practical phased-array-based IRS and avoiding the complexity associated with TTD-enabled implementations. Finally, compared to max–min beamforming schemes [48], [49], which maximize the minimum array gain across SCs, the achieved gain by them is significantly lower than the peak array gain, reflecting the fundamental limitation of optimizing a single phase-shifter-based IRS configuration jointly over a wide BW. Note that optimizing the IRS to $f_n = 0$ produces deep nulls in the channel gain, which the max–min beamforming solution is able to avoid, but at the cost of a lower channel gain across the BW. In summary, the proposed approach provides an effective solution for wideband IRS beamforming.

Next, in Fig. 9, we evaluate the system throughput as a function of the number of UEs, K, for scenarios $(1), (2)$, and (4), outlined in the previous paragraph. In the RR case, the rate falls short of the ideal scaling $\mathcal{O}(\log_2(M^2))$ due to the B-SP effect and remains constant with increasing K, since RR scheduling does not exploit multi-user diversity. In contrast, with a max-rate scheduler, the rate increases with K because it *opportunistically* schedules the UEs with better channel conditions. In the absence of channel fading, the throughput exceeds that achieved under RR scheduling with as few as 20

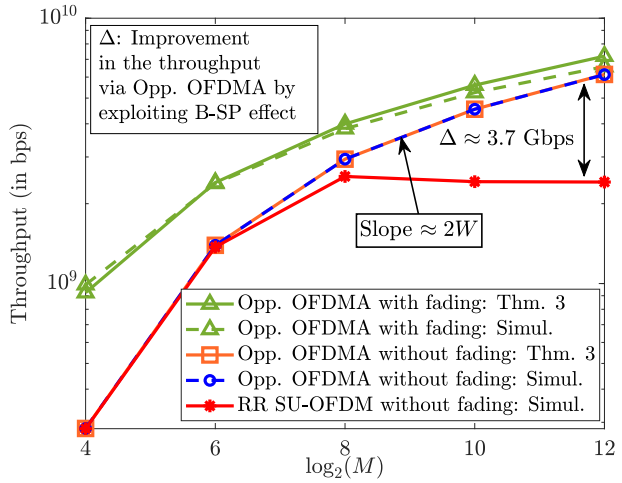

Fig. 10: Throughput vs. No. of IRS elements, M, for $K = 5000$.

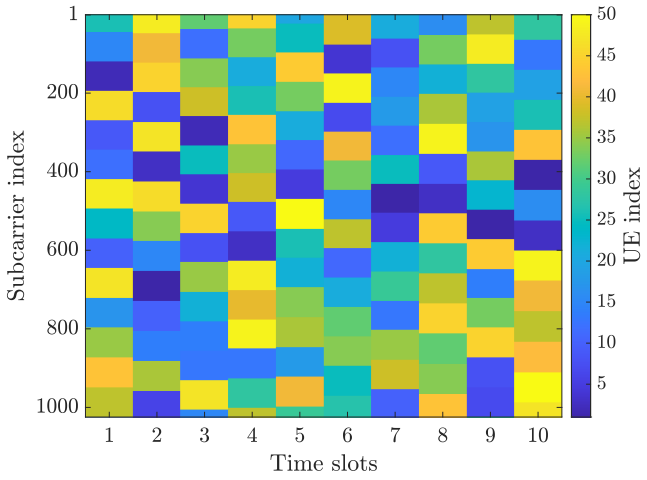

Fig. 11: UE Scheduling over OFDM resource grid. $\mathcal{R} = [75°, 90°]$.

UEs and gradually converges to the optimal rate scaling of $\mathcal{O}(\log_2(M^2))$ for larger values of K (in fact, just $K = 200$ UEs are sufficient), in line with Theorem 2. When channel fading is present, multi-user diversity yields an additional gain, improving the rate to $\mathcal{O}(\log_2(M^2 \ln K))$, as predicted by Theorem 3. These results demonstrate that by leveraging the B-SP effect and employing opportunistic scheduling across the SCs with multiple UEs, the proposed scheme achieves near-optimal performance on all SCs simultaneously.

Next, in Fig. 10, we evaluate the effectiveness of the proposed scheme by plotting the system throughput versus the number of IRS elements (on a log-scale) for the three scenarios. For small M, all curves exhibit a slope of $2W$, indicating that the full array gain of M^2 is realized across all SCs spanning a BW of W. However, as M increases, the B-SP effect becomes significant, causing the slope of the RR scheduler curve to fall below $2W$. In contrast, the slope remains close to $2W$ for the max-rate scheduling scenarios, confirming that the full array gain from the IRS is retained across all SCs by exploiting the B-SP effect via opportunistic scheduling. The vertical offsets between the curves with and without fading reflect the additional rate gains from multi-user diversity in the presence of fading, which scale as $\mathcal{O}(\log \ln K)$.

Finally, Fig. 11 illustrates a heatmap of UE scheduling across time slots and SC frequencies, where each color corresponds to the index of the UE scheduled on the associated time-frequency resource. For this experiment, we consider 1024 SCs and 10 time slots and perform opportunistic OFDMA over 50 UEs within the area. Through this plot, we make the following two observations:

1) **Fairness over time**: Every UE within the angular coverage region is scheduled over time, i.e., the scheduler is fair across the UEs. Primarily, this is because the sampling distribution of the IRS is designed to reflect signals to all possible UE directions over time, and the BS schedules UEs whose channels are best aligned with the IRS beam.
2) **Contiguous SC allocation at a UE**: A given UE is scheduled on a contiguous set of SCs. Hence, (a) a UE only needs to extract data symbols on a contiguous set of SCs for further decoding, and not on any other isolated SCs within the BW; (b) the channel gain at a UE on the SCs on which it is scheduled is nearly equal; (c) the signaling overhead for channel state information (CSI) feedback from the UEs can be reduced, because the UEs only need to convey the start and end indices of the SCs where they observe high CSI; (d) similarly, the overhead in downlink control information (DCI) channels where the SC allocation is conveyed to the UE can also be reduced.

Thus, the proposed method is fair across all users and has low complexity, making it attractive for practical implementation.

VI. Conclusions

In this paper, we demonstrated that the B-SP effect, which is typically considered a limitation in IRS-aided wideband systems, can instead be harnessed to enhance the system performance. We first established that, under the B-SP effect, the IRS exhibits a multi-directional beamforming property, which enables the IRS to focus its reflected energy toward different spatial directions on different SCs. Exploiting this property of the B-SP effect, we showed that by employing an OFDMA framework with a max-rate scheduling policy, it is possible to almost surely achieve the full array gain of the IRS on all SCs, provided a sufficiently large number of UEs are present in the system. We then derived the corresponding rate scaling laws and proved that the proposed scheme not only achieves the optimal beamforming gain over the entire BW, but also benefits from multi-user diversity, leading to further performance enhancements. Finally, we discussed how the idea extends to near-field systems and its low-overhead nature. Future directions include integrating fairness-aware UE scheduling, addressing quality-of-service requirements, accounting for hardware impairments, extension to hybrid near-far field cases [50], analysis with UE mobility, etc.

VII. Acknowledgement

We thank Siddhartha Parupudi (IIT Delhi, India) for the helpful discussions during the initial part of this work.

REFERENCES

[1] P. Siddhartha, L. Yashvanth, and C. R. Murthy, "Exploiting beam-split in IRS-aided systems via OFDMA," in *Proc. IEEE Int. Conf. Acoust., Speech Signal Process. (ICASSP)*, Apr. 2025, pp. 1–5.

[2] E. Basar, M. Di Renzo, J. De Rosny, M. Debbah, M.-S. Alouini, and R. Zhang, "Wireless communications through reconfigurable intelligent surfaces," *IEEE Access*, vol. 7, pp. 116 753–116 773, 2019.

[3] E. Björnson *et al.*, "Reconfigurable intelligent surfaces: A signal processing perspective with wireless applications," *IEEE Signal Process. Mag.*, vol. 39, no. 2, pp. 135–158, Mar. 2022.

[4] Y. Cao *et al.*, "Intelligent reflecting surface aided multi-user mmwave communications for coverage enhancement," in *Proc. IEEE 31st Annu. Int. Symp. Pers., Indoor Mobile Radio Commun.*, Aug. 2020, pp. 1–6.

[5] M. Nemati *et al.*, "RIS-assisted coverage enhancement in millimeter-wave cellular networks," *IEEE Access*, vol. 8, pp. 188 (171–185), 2020.

[6] B. Wang, F. Gao, S. Jin, H. Lin, and G. Y. Li, "Spatial- and frequency-wideband effects in millimeter-wave massive MIMO systems," *IEEE Trans. Signal Process.*, vol. 66, no. 13, pp. 3393–3406, Jul. 2018.

[7] X. Ye *et al.*, "Joint codebook selection and MCS adaptation for mmwave eMBB services based on deep reinforcement learning," *IEEE Internet of Things Journal*, vol. 11, no. 19, pp. 31 545–31 560, Oct. 2024.

[8] P. Wang *et al.*, "Intelligent reflecting surface-assisted millimeter wave communications: Joint active and passive precoding design," *IEEE Trans. Veh. Technol.*, vol. 69, no. 12, pp. 14 960–14 973, Dec. 2020.

[9] W. Mei *et al.*, "Intelligent reflecting surface-aided wireless networks: From single-reflection to multireflection design and optimization," *Proceedings of the IEEE*, vol. 110, no. 9, pp. 1380–1400, Sep. 2022.

[10] H. Sun, S. Zhang, J. Ma, and O. A. Dobre, "Time-delay unit based beam squint mitigation for RIS-aided communications," *IEEE Commun. Lett.*, vol. 26, no. 9, pp. 2220–2224, Sep. 2022.

[11] R. Su *et al.*, "Wideband precoding for RIS-aided THz communications," *IEEE Trans. Commun.*, vol. 71, no. 6, pp. 3592–3604, Jun. 2023.

[12] H. L. Van Trees, *Optimum array processing: Part IV of detection, estimation, and modulation theory*. John Wiley & Sons, 2002.

[13] S. Ma, W. Shen, J. An, and L. Hanzo, "Wideband channel estimation for IRS-aided systems in the face of beam squint," *IEEE Trans. Wireless Commun.*, vol. 20, no. 10, pp. 6240–6253, Oct. 2021.

[14] A. Abdallah *et al.*, "Deep-learning based channel estimation for RIS-aided mmwave systems with beam squint," in *Proc. IEEE Int. Conf. Commun.*, May 2022, pp. 1269–1275.

[15] K. Keykhosravi *et al.*, "RIS-enabled SISO localization under user mobility and spatial-wideband effects," *IEEE J. Sel. Topics Signal Process.*, vol. 16, no. 5, pp. 1125–1140, Aug. 2022.

[16] Y. Chen *et al.*, "Beam-squint mitigating in reconfigurable intelligent surface aided wideband mmwave communications," in *Proc. IEEE Wireless Commun. Netw. Conf. (WCNC)*, Mar. 2021, pp. 1–6.

[17] Y. Jiang *et al.*, "Beamforming design for RIS-aided THz wideband communication systems," in *Proc. IEEE 24th Int. Workshop Signal Process. Adv. Wireless Commun. (SPAWC)*, Sep. 2023, pp. 296–300.

[18] J. Wu and B. Shim, "Frequency-dependent beamforming for RIS-assisted wideband terahertz systems," in *2023 IEEE 97th Vehicular Technology Conference (VTC2023-Spring)*, Jun. 2023, pp. 1–6.

[19] R. Li *et al.*, "Ergodic achievable rate maximization of RIS-assisted millimeter-wave MIMO-OFDM communication systems," *IEEE Trans. Wireless Commun.*, vol. 22, no. 3, pp. 2171–2184, Mar. 2023.

[20] H. Ozen and G. M. Guvensen, "A robust quantized beam-squint and interference aware statistical beamforming for RIS-aided massive MIMO," in *Proc. IEEE Int. Conf. Commun.*, May 2023, pp. 1307–1312.

[21] Y. Kawamoto *et al.*, "Simultaneous multiple connections and increased frequency efficiency using beam squint approach for IRS-based communication," *IEEE Trans. Veh. Technol.*, vol. 73, no. 11, pp. 17 073–17 082, Nov. 2024.

[22] W. Hao *et al.*, "The far-/near-field beam squint and solutions for THz intelligent reflecting surface communications," *IEEE Trans. Veh. Technol.*, vol. 72, no. 8, pp. 10 107–10 118, Aug. 2023.

[23] F. Zhao *et al.*, "Joint beamforming optimization for IRS-aided THz communication with time delays," *IEEE Wireless Commun. Lett.*, vol. 13, no. 1, pp. 49–53, Jan. 2024.

[24] Z. Zhang, L. Dai, X. Chen, C. Liu, F. Yang, R. Schober, and H. V. Poor, "Active RIS vs. passive RIS: Which will prevail in 6G?" *IEEE Trans. Commun.*, vol. 71, no. 3, pp. 1707–1725, Mar. 2023.

[25] M. Ma, N. T. Nguyen, and M. Juntti, "Beam squint analysis and mitigation via hybrid beamforming design in THz communications," in *Proc. IEEE Int. Conf. Commun. (ICC)*, May 2023, pp. 6486–6491.

[26] L. Yashvanth, C. R. Murthy, and B. D. Rao, "Mitigating spatial-wideband and beam-split effects via distributed IRSs: Design and analysis," *IEEE Trans. Signal Process.*, vol. 73, pp. 3286–3301, 2025.

[27] B. Zheng, C. You, and R. Zhang, "Intelligent reflecting surface assisted multi-user OFDMA: Channel estimation and training design," *IEEE Trans. Wireless Commun.*, vol. 19, no. 12, pp. 8315–8329, Dec. 2020.

[28] Y. Yang, S. Zhang, and R. Zhang, "IRS-enhanced OFDMA: Joint resource allocation and passive beamforming optimization," *IEEE Wireless Commun. Lett.*, vol. 9, no. 6, pp. 760–764, Jun. 2020.

[29] S. Ma, W. Shen, J. An, and L. Hanzo, "Wideband channel estimation for IRS-aided systems in the face of beam squint," *IEEE Trans. Wireless Commun.*, vol. 20, no. 10, pp. 6240–6253, Oct. 2021.

[30] Z. Wan, Z. Gao, and M.-S. Alouini, "Broadband channel estimation for intelligent reflecting surface aided mmwave massive MIMO systems," in *Proc. IEEE Int. Conf. Commun. (ICC)*, Jun. 2020, pp. 1–6.

[31] L. Yashvanth and C. R. Murthy, "On the impact of an IRS on the out-of-band performance in sub-6 GHz and mmwave frequencies," *IEEE Trans. Commun.*, vol. 72, no. 12, pp. 7417–7434, Dec. 2024.

[32] J. Chen *et al.*, "Channel estimation for reconfigurable intelligent surface aided multi-user mmwave MIMO systems," *IEEE Trans. Wireless Commun.*, vol. 22, no. 10, pp. 6853–6869, Oct. 2023.

[33] G. Lee, Y. Sung, and J. Seo, "Randomly-directional beamforming in millimeter-wave multiuser MISO downlink," *IEEE Trans. Wireless Commun.*, vol. 15, no. 2, pp. 1086–1100, Feb. 2016.

[34] J. Li, S. Zhang, Z. Li, J. Ma, and O. A. Dobre, "User sensing in RIS-aided wideband mmwave system with beam-squint and beam-split," *IEEE Trans. Commun.*, vol. 73, no. 2, pp. 1304–1319, Feb. 2025.

[35] L. Yashvanth and C. R. Murthy, "Performance analysis of intelligent reflecting surface assisted opportunistic communications," *IEEE Trans. Signal Process.*, vol. 71, pp. 2056–2070, 2023.

[36] H. Sun, L. Zhu, W. Mei, and R. Zhang, "Power-measurement-based channel autocorrelation estimation for IRS-assisted wideband communications," *IEEE Trans. Wireless Commun.*, vol. 24, no. 6, pp. 4647–4662, Jun. 2025.

[37] L. Yashvanth, C. R. Murthy, and B. D. Rao, "Spatial correlation-aware opportunistic beamforming in IRS-aided multi-user systems," *IEEE Wireless Commun. Lett.*, vol. 14, no. 10, pp. 3174–3178, Oct. 2025.

[38] G. Grimmett and D. Stirzaker, *Probability and random processes*, 3rd ed. Oxford university press, 2001.

[39] L. Yashvanth and C. R. Murthy, "Comparative study of IRS assisted opportunistic communications over i.i.d. and LoS channels," in *Proc. IEEE Int. Conf. Acoust., Speech Signal Process. (ICASSP)*, Jun. 2023.

[40] N. H. Mahmood *et al.*, "Machine type communications: Key drivers and enablers towards the 6G era," *EURASIP Journal on Wireless Communications and Networking*, vol. 2021, no. 1, p. 134, 2021.

[41] Q.-U.-A. Nadeem *et al.*, "Intelligent reflecting surface enabled random rotations scheme for the MISO broadcast channel," *IEEE Trans. Wireless Commun.*, vol. 20, no. 8, pp. 5226–5242, Aug. 2021.

[42] P. Viswanath, D. Tse, and R. Laroia, "Opportunistic beamforming using dumb antennas," *IEEE Transactions on Information Theory*, vol. 48, no. 6, pp. 1277–1294, 2002.

[43] Q. Yu and L. Dai, "Near-field wideband beamforming for RIS based on fresnel zones," *IEEE Trans. Commun.*, vol. 73, no. 7, pp. 5126–5138, Jul. 2025.

[44] H. Luo, F. Gao, W. Yuan, and S. Zhang, "Beam squint assisted user localization in near-field integrated sensing and communications systems," *IEEE Trans. Wireless Commun.*, vol. 23, no. 5, pp. 4504–4517, May 2024.

[45] M. Cui and L. Dai, "Channel estimation for extremely large-scale MIMO: Far-field or near-field?" *IEEE Trans. Commun.*, vol. 70, no. 4, pp. 2663–2677, Apr. 2022.

[46] V. Shah *et al.*, "Optimal timer based selection schemes," *IEEE Trans. Commun.*, vol. 58, no. 6, pp. 1814–1823, Jun. 2010.

[47] "3GPP Rep. TR 38.901 V16.1.0: Study on channel model for frequencies from 0.5 to 100 GHz," *3GPP, Sophia Antipolis, France*, Dec. 2019.

[48] D. Wang, W. Mei, Z. Chen, and B. Ning, "Performance analysis and reflection optimization for wideband THz double-IRS aided wireless communications," in *Proc. IEEE Int. Conf. Commun. (ICC)*, Jun. 2024, pp. 2519–2524.

[49] B. Ning, W. Mei, L. Zhu, Z. Chen, and R. Zhang, "Codebook design and performance analysis for wideband beamforming in terahertz communications," *IEEE Trans. Wireless Commun.*, vol. 23, no. 12, pp. 19 618–19 633, Dec. 2024.

[50] Y. Li and A. S. Madhukumar, "Hybrid near- and far-field THz UM-MIMO channel estimation: A sparsifying matrix learning-aided bayesian approach," *IEEE Trans. Wireless Commun.*, vol. 24, no. 3, pp. 1881–1897, Mar. 2025.

L. Yashvanth received the B. Tech (Hons.) degree in Electronics and Communication Engineering from National Institute of Technology, Trichy, India, with a gold medal in 2020 and an integrated Ph. D. degree from the Indian Institute of Science, Bangalore, in 2025. Currently, he is a research fellow at University College London, U.K. His broad areas of research interests include statistical signal processing and its applications to 5G and next-generation wireless communication systems. He is a recipient of a DAAD-WISE fellowship in 2019, Qualcomm Innovation Fellowship in 2021 and 2022, and the Prime Minister's Research Fellowship (PMRF), Govt. of India in 2022. He also won the Best Poster Presentation award at the PMRF Symposium held at IIT Indore in 2024, and the Prof. Satish Dhawan Research Award in 2025 for impactful research in the Division of EECS at IISc, Bangalore.

Chandra R. Murthy (S'03–M'06–SM'11–F'23) received the B. Tech. degree in Electrical Engineering from the Indian Institute of Technology Madras, India, in 1998, the M. S. and Ph. D. degrees in Electrical and Computer Engineering from Purdue University and the University of California, San Diego, USA, in 2000 and 2006, respectively. In Sept. 2007, he joined the Department of Electrical Communication Engineering at the Indian Institute of Science, Bangalore, India, where he is currently working as a Professor.

From 2000 to 2002, he was with Qualcomm Inc., on WCDMA baseband transceiver design and 802.11b baseband receivers. From 2006 to 2007, he was a Staff Engineer with Beceem Communications Inc., on advanced receiver architectures for the 802.16e mobile WiMAX standard. His research interests are in the areas of sparse signal recovery, energy harvesting-based communication, performance analysis, and optimization of 5G and beyond communications. Papers co-authored by him have received Student/Best Paper Awards at the NCC 2014, IEEE ICASSP 2018, IEEE ISIT 2021, IEEE SPAWC 2022, and NCC 2023. He has served on the editorial board of the IEEE SIGNAL PROCESSING LETTERS, IEEE TRANSACTIONS ON SIGNAL PROCESSING, SADHANA Journal, and the IEEE TRANSACTIONS ON COMMUNICATIONS. Currently, he is an elected member of the IEEE SAM Technical Committee and a Senior Area Editor of the IEEE TRANSACTIONS ON INFORMATION THEORY. He is a fellow of the IEEE and INAE.